Study of DNA binding and bending by Bacillus subtilis GabR, a PLP-dependent transcription factor

Elsevier Editorial System(tm) for BBA - General Subjects

Manuscript Draft

Manuscript Number: BBAGEN-16-566R1

Title: Study of DNA binding and bending by Bacillus subtilis GabR, a PLP-dependent transcription factor

Article Type: Regular Paper

Keywords: Transcription factor
MocR
GABA metabolism
PLP enzyme
Atomic Force Microscopy

Corresponding Author: Prof. Claudio Rivetti,

Corresponding Author's Institution: University of Parma

First Author: Davide Amidani

Order of Authors: Davide Amidani; Angela Tramonti; Andrea Valeria Canosa; Barbara Campanini; Stefano Maggi; Teresa Milano; Martino L di Salvo; Stefano Pascarella; Roberto Contestabile; Stefano Bettati; Claudio Rivetti

Abstract: Background: GabR is a transcriptional regulator belonging to the MocR/GabR family, characterized by a N-terminal wHTH DNA-binding domain and a C-terminal effector binding and/or oligomerization domain, structurally homologous to aminotransferases (ATs). In the presence of γ-aminobutyrate (GABA) and pyridoxal 5'-phosphate (PLP), GabR activates the transcription of gabT and gabD genes involved in GABA metabolism.

Methods: Here we report a biochemical and atomic force microscopy characterization of Bacillus subtilis GabR in complex with DNA. Complexes were assembled in vitro to study their stoichiometry, stability and conformation.

Results: The fractional occupancy of the GabR cognate site suggests that GabR binds as a dimer with Kd of 10 nM. Upon binding GabR bends the DNA by 80° as measured by anomalous electrophoretic mobility. With GABA we observed a decrease in affinity and conformational rearrangements compatible with a less compact nucleo-protein complex but no changes of the DNA bending angle. By employing promoter and GabR mutants we found that basic residues of the positively charged groove on the surface of the AT domain affect DNA affinity.

Conclusions: The present data extend current understanding of the GabR-DNA interaction and the effect of GABA and PLP. A model for the GabR-DNA complex, corroborated by a docking simulation, is proposed.

General Significance: Characterization of the GabR DNA binding mode highlights the key role of DNA bending and interactions with bases

outside the canonical direct repeats, and might be of general relevance for the action mechanism of MocR transcription factors.

Response to Reviewers: First, we thank the reviewer for their valuable comments which helped to improve the quality of the manuscript.

Response to Reviewer #1 comment No. 1:
As shown in table 1 (compare data in rows 1 and 2), we do observe small changes of the conformation of the complexes upon the addition of GABA: in the presence of GABA the complexes have a smaller image profile and a larger surface area. On the other hand the volume is not significantly different but confirms the dimeric form of GabR. Moreover, a twofold increase of the Kd is observed in the presence of GABA. A footprinting analysis of GabR with and without GABA has been carried out previously (Belitsky 2004). In that study the authors concluded that: "Addition of GABA together with PLP did not noticeably alter the pattern of GabR-mediated protection and decreased the strength of GabR-DNA interaction about twofold … ". Our speculation regarding the possibility that GabR may favor open promoter complex formation arises from the consideration that a simple derepression mechanism cannot be accounted for by the small changes in Kd. It is possible that small conformational changes, not detected by AFM and DNA footprinting, can switch the regulatory activity of this interesting protein.

Response to Reviewer #1 comment No. 2:
Based on this reviewer suggestion we have performed additional electrophoretic mobility shift assays to determine the effect of 5 and 10 bp insertion on the migration. Unfortunately the observed differences in migration are not really relevant, and although we can determine a smaller bend angle value for the 5Ins we do not feel confident on such small variation. Therefore we have removed from the manuscript any conclusion derived from the migration of free DNA.
A description of the procedure used to predict DNA curvature has been added to the Materials and Methods. The url of the web service is now provided.

Response to Reviewer #2 comment No. 1:
We have re-arranged the position of relevant references in the introduction and reworded some sentences to address this concern.
We are aware that this is not a breakthrough article, however, in our opinion, the manuscript contains several original data:
- the first AFM investigation of GabR/DNA interaction.
- the first determination of the DNA bend angle induced by GabR.
- the first attempt to identify AT domain residues involved in DNA interaction.
- the first analysis of apo-GabR/DNA interaction.

Response to Reviewer #2 comment No. 2:
The approach presented here represents a conventional method that has been applied many times to PLP-dependent enzymes to assess the formation of a covalent bond between the cofactor and the protein. In fact, PLP binds to PLP-dependent enzymes forming an imine (more commonly indicated as a Schiff base) which is labile in aqueous solutions (Cordes 1962; Burger et al. 1981). In addition to the covalent imine linkage the interaction of PLP with its binding site within proteins is also stabilized by many additional non-covalent interactions. As long as the protein retains its native structure the cofactor is quite firmly bound

to the protein. However, after denaturation, the Schiff base can undergo hydrolysis (Hughes 1962). The interaction of PLP with the protein can be stabilized by a reduction of the Schiff base to a secondary amine (Hughes 1962; Simon 2009) by means of $NaNH_4$. The formation of an amine between the enzyme and PLP is proven spectroscopically by the disappearance of the typical visible band of the internal aldimine (400-425 nm, depending on the enzyme/protein) and the accumulation of a species absorbing at around 335 nm (Hughes 1962), which is the substituted amine. The same reduction also takes place on the so-called external aldimines, i.e. the product of a transaldimination reaction between protein-bound PLP and amine. However, when this iminic bond is reduced, a stable covalent bond is formed between PLP and the free amino acid. Denaturation and dialysis thus lead to the removal of PLP from the protein.
As suggested by this reviewer, we added a new paragraph in Materials and Methods with a detailed description of this methodology and some additional references. A control spectrum of denatured GabR without reduction has been added to Supplementary Figure 1A. We also introduced changes in the Results section to better explain the usefulness of this method to differentiate between internal and external aldimine.

Response to Reviewer #2 comment No. 3:
This behavior of GabR is consistent with data obtained in vivo using gabT, gabD and gabR null mutants as first demonstrated by Belitsky et al 2002. Further references to this and other studies have been added.

Response to Reviewer #2 comment No. 4:
Our conclusion that "DNA bending controls binding of GabR" may be an over interpretation of the data since our DNA binding site mutants contain changes of the wild-type sequence. However, it is difficult to change/remove DNA bending without altering the DNA sequence. For this reason, in the Results and Discussion sections we always interpret our results in terms of DNA bending and phasing. The interesting result is not just the loss of binding after an insertion of five bp but the fact that binding and bending are almost completely recovered with an insertion of ten bp. This said, we do understand the reviewer's concern about the title of the manuscript which may not entirely reflect the reported results. Therefore we have changed the title of the manuscript as follows: "Study of DNA binding and bending by Bacillus subtilis GabR, a PLP-dependent transcription factor".

Response to Reviewer #2 comment No. 5:
This sentence has been rephrased as follows: "By employing promoter and GabR mutants we found that basic residues of the positively charged groove on the surface of the AT domain affect DNA affinity."

Response to Reviewer #2 comment No. 6:
We have used the position of the protein along the DNA template to assess the specificity of the complexes since this procedure is widely used in the field of protein/DNA investigation by single molecule visualization techniques (AFM and EM). Of course, given the "low" lateral resolution of the AFM microscope (few nanometers) we cannot discriminate between proteins bound to the DNA with an offset of ten or less base pairs with respect to the cognate binding site boundaries. In this regard, EMSA assays, widely used to determine binding affinities and DNA bending, do not guarantee that the band shift is determined only by specific complexes even if heparin or filler DNA is add to the reaction. In our 20-year experience in AFM imaging, GabR is the transcription factor that

shows the highest specificity for its binding site. No other protein studied by us has such a high ratio of specific vs aspecific complexes.

Response to Reviewer #2 comment No. 7:
True. This manuscript reports an in vitro study of the GabR-DNA interaction. The in vivo characterization of these GabR mutants is part of follow-up work.

Response to Reviewer #2 comment No. 8:
In the introduction we now provide a definition of Schiff-base. Reduced Schiff base refers to a Schiff base where the double bond has been reduced to a substituted amine. However, to avoid any ambiguity, throughout the text we refer to this species as substituted amine (see also Hughes, 1962).

Response to Reviewer #2 comment No. 9:
Corrected.

Response to Reviewer #2 comment No. 10:
Reference to Buell and Hansen 1960 has been added.

Response to Reviewer #3 comment No. 1:
Corrected.

Response to Reviewer #3 comment No. 2:
This sentence has been deleted.

Cover Letter

Dear Editor,

I am submitting the revised version of the manuscript with reference No. BBAGEN-16-566 to be considered for publication in BBA General Subjects. Changes to the text have been made accordingly to the reviewers' comments. To facilitate the reviewing process changes to the text are in red. Please note that in order to fulfill reviewer #2 concerns, we have changed the title of the manuscript. The new title is: "Study of DNA binding and bending by Bacillus subtilis GabR, a PLP-dependent transcription factor".

Thank you for the consideration given to this manuscript.

I look forward to hear from you.

Sincerely,
Claudio Rivetti

Graphical Abstract (for review)

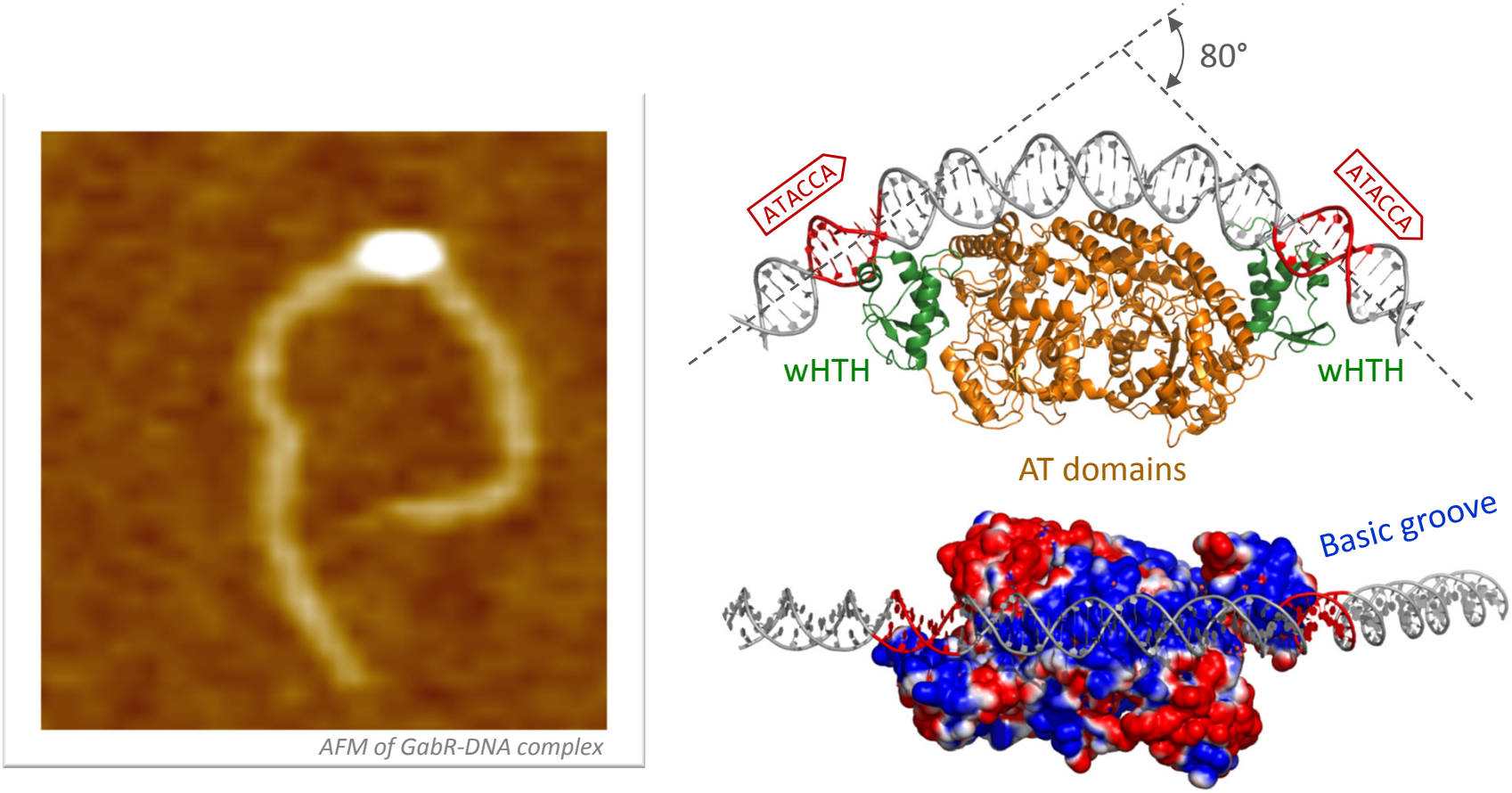

HIGHLIGHTS

- GabR binds two DNA direct repeats as a dimer and bends the cognate site by ~80°.
- Proper phasing of direct repeats is crucial for GabR binding.
- PLP is not required for the GabR-DNA interaction.
- GABA reduces GabR-DNA affinity and alters slightly the shape of the complexes.
- Basic residues of the AT domain affect GabR-DNA binding affinity.

Study of DNA binding and bending by *Bacillus subtilis* GabR, a PLP-dependent transcription factor

Davide Amidani[1], Angela Tramonti[2,3], Andrea Valeria Canosa[4], Barbara Campanini[4], Stefano Maggi[1], Teresa Milano[3], Martino L. di Salvo[3], Stefano Pascarella[3], Roberto Contestabile[3], Stefano Bettati[5,6] and Claudio Rivetti[1]*

[1] Dipartimento di Bioscienze, Università degli Studi di Parma, Parma, Italy

[2] Istituto di Biologia e Patologia Molecolari, Consiglio Nazionale delle Ricerche, Roma, Italy

[3] Dipartimento di Scienze Biochimiche 'A. Rossi Fanelli', Sapienza Università di Roma, Italy

[4] Dipartimento di Farmacia, Università di Parma, Parma, Italy

[5] Dipartimento di Neuroscienze, Università di Parma, Parma, Italy

[6] National Institute of Biostructures and Biosystems, Rome, Italy

* To whom correspondence should be addressed. Tel: +39 0521 905650; Fax: +39 0521 905151;
Email: claudio.rivetti@unipr.it

Abstract

Background: GabR is a transcriptional regulator belonging to the MocR/GabR family, characterized by a N-terminal wHTH DNA-binding domain and a C-terminal effector binding and/or oligomerization domain, structurally homologous to aminotransferases (ATs). In the presence of ɔ-aminobutyrate (GABA) and pyridoxal 5'-phosphate (PLP), GabR activates the transcription of *gabT* and *gabD* genes involved in GABA metabolism.

Methods: Here we report a biochemical and atomic force microscopy characterization of *Bacillus subtilis* GabR in complex with DNA. Complexes were assembled *in vitro* to study their stoichiometry, stability and conformation.

Results: The fractional occupancy of the GabR cognate site suggests that GabR binds as a dimer with *K*d of 10 nM. Upon binding GabR bends the DNA by 80° as measured by anomalous electrophoretic mobility. With GABA we observed a decrease in affinity and conformational rearrangements compatible with a less compact nucleo-protein complex but no changes of the DNA bending angle. By employing promoter and GabR mutants we found that basic residues of the positively charged groove on the surface of the AT domain affect DNA affinity.

Conclusions: The present data extend current understanding of the GabR-DNA interaction and the effect of GABA and PLP. A model for the GabR-DNA complex, corroborated by a docking simulation, is proposed.

General Significance: Characterization of the GabR DNA binding mode highlights the key role of DNA bending and interactions with bases outside the canonical direct repeats, and might be of general relevance for the action mechanism of MocR transcription factors.

1. Introduction

GabR is a transcription factor widespread in eubacteria, belonging to the GntR family and the MocR/GabR subfamily [1-3]. GabR controls the expression of the *gabTD* operon for the utilization of γ-aminobutyric acid (GABA), which is also the allosteric effector, as nitrogen and carbon source. In *Bacillus subtilis*, the *gabT* and *gabD* genes encode for two enzymes required for an alternative route of glutamate biosynthesis using GABA [1]. GabT is a fold-type I aminotransferase (AT) that catalyzes the transamination of GABA to form succinic semialdehyde and glutamate, while GabD is a NAD-dependent dehydrogenase that converts succinic semialdehyde to succinate.

B. subtilis GabR is a chimeric protein composed by a N-terminal winged helix-turn-helix (wHTH) DNA-binding domain and a C-terminal domain characteristic of the fold type I pyridoxal 5'-phosphate (PLP)-dependent AT family. The two domains are connected by a 29 amino acids long flexible linker. The invariant lysine K312 of the C-terminal domain forms an imine with PLP (Schiff base), also referred to as internal aldimine [4]. Although the GabR C-terminal domain has sequence similarity with functional ATs [4, 5], structural features of the active site, namely the lack of space and interactions required to accommodate both GABA and an α-ketoacid , suggest that GabR cannot catalyze the aminotransferase reaction, leading only to the formation of an external aldimine between GABA and PLP [5]. Both *in vivo* and *in vitro* experiments have demonstrated that PLP and GABA are required to activate the *gabT* and *gabD* genes [1, 5, 6], thus suggesting that GabR acts as a PLP-dependent transcriptional activator using GABA as an allosteric modulator. *In vitro* DNA binding assays showed that binding of GABA to the AT domain does not release the regulator from the promoter [5-7], but rather it switches GabR from being a repressor to an activator of the *gabTD* operon [6]. GabR can also regulate its own transcription behaving as a GABA-independent negative autoregulator [1].

GabR crystallizes as a homodimer with the two monomers organized in a head-to-tail domain-swap arrangement, in which the wHTH domain of one subunit makes contacts with the AT domain of the other subunit [4]. The specific interaction of GabR with DNA occurs within an extended region of 47 bp that overlaps the -35 and -10 elements of the *gabTD* and *gabR* divergent promoters, respectively [6]. The DNA sequence protected by GabR contains two ATACCA direct repeats separated by a 29 bp long spacer. The interaction with direct repeats is uncommon in prokaryotic homodimeric transcription factors, however the characteristic quaternary structure of MocR family members might accommodate this particular binding architecture [2, 8]. For instance, the MocR member *Rhodobacter capsulatus* TauR, involved in taurine metabolism, specifically recognizes direct repeats [9]. Moreover, the GabR homolog transcriptional regulator PdxR from *Bacillus clausii*, which activates transcription of the *pdxST* gene encoding PLP synthase, can bind either direct or inverted repeats in the promoter region depending on the presence or absence of PLP [10].

Based on the GabR crystal structure, Edayathumangalam and colleagues proposed two different models for GabR-DNA binding: one assumes that a dimer of dimers binds the target sequence, whereby only one wHTH domain of each dimer contacts one of the two ATACCA direct repeats; the other assumes that a single GabR

dimer binds the entire target sequence, through a one-to-one interaction of the wHTH domains with the direct repeats [4]. In support of the latter mode of interaction, a recent SAXS study has shown that GabR binds the two direct repeats of the cognate site as a dimer, and a model was proposed suggesting that the bendability of the promoter region plays a key role in the stability of the complex [7].

With the aim to better comprehend the DNA binding mode of this regulator and to gather further insights into the allosteric mechanism of gene regulation of *B. subtilis* GabR, we employed Atomic Force Microscopy (AFM) and electrophoretic mobility shift assays (EMSA) to study the stoichiometry, conformation and stability of GabR-DNA specific complexes, and the effect of PLP and GABA on this interaction. Analysis of promoter mutants suggests that not only the ATACCA direct repeats, but also nucleotides of the intervening DNA spacer play an important role in the interaction. In agreement with SAXS data, our results show that bending of the promoter DNA and proper phasing of the DNA binding sites are required for GabR binding. Upon binding, GabR bends the DNA by ~80°. Furthermore, point mutations in the AT domain of GabR show that the positively charged groove found on the surface of the protein is a key determinant of the specific recognition of the promoter and highlights the direct role played by this domain in the protein-DNA interaction. While PLP has little or no effect on the DNA binding affinity, GABA affects both the stability and the conformation of the complex, suggesting a possible action mechanism of the GabR transcription factor. Overall, our data emphasize the complexity of the DNA sequence recognized by GabR and provide an example of a mechanism where the shape and charge complementarity of an extended portion of the protein-DNA interface are required for the specific recognition of the DNA target site.

2. Materials and Methods

2.1. Cloning, expression and purification of wild-type and mutant GabR

The genomic DNA of *Bacillus subtilis* strain WB800N was purified as described in [11].

GabR coding sequence was amplified by PCR using Taq DNA polymerase with primers GabR-for and GabR-rev (Supplementary Table 1) in standard reaction conditions. The amplicon was digested with BsaI restriction enzyme and ligated to a linearized pASK-IBA3 plus vector (IBA, Göttingen, Germany) with compatible ends. This vector adds a *Strep-tag II* to the GabR C-terminus. The pASK-GabR construct was verified by DNA sequencing and used to transform *E. coli* BL21(DE3) competent cells.

10 ml of an overnight cell culture were then used to inoculate 500 ml of LB medium containing 100 µg/ml ampicillin. Cells were grown at 37 °C for 3 h (OD_{600} = 0.6). GabR expression was induced with the addition of 200 ng/ml anhydrotetracycline and the culture was grown at 30 °C for other 3 h. Culture was harvested at 4 °C and the pellet was resuspended in lysis buffer (50 mM NaH_2PO_4 pH 8, 300 mM NaCl, 0.2 mM PLP, 1 mM DTT, 1 mM EDTA, 0.2 mM protease inhibitor PMSF (Sigma Aldrich)). Cell lysis was performed by sonication on ice. The cell homogenate was centrifuged at 13,000 x *g* for 45 min. at 4 °C. The supernatant was loaded onto a Strep-Tactin column (IBA, Göttingen, Germany) pre-equilibrated with lysis buffer. The column was washed with five bed volumes of wash buffer (50 mM NaH_2PO_4 pH 8, 300 mM NaCl, 1 mM DTT, 1 mM EDTA). The protein was eluted with 3 ml of elution buffer (50 mM NaH_2PO_4 pH 8, 300 mM NaCl, 1 mM DTT, 1 mM EDTA, 2.5 mM desthiobiotin). After addition of a 10X PLP molar excess, the protein solution was dialyzed overnight at 4 °C against storage buffer (50 mM NaH_2PO_4 pH 8, 300 mM NaCl, 1 mM EDTA). GabR purity was verified by SDS-PAGE and the concentration was determined from the absorbance at 280 nm using an extinction coefficient of 53290 M^{-1} cm^{-1}. Glycerol to a final concentration of 15% v/v was added and GabR was stored at -80 °C.

The R129Q and K362.366Q GabR mutants were obtained with the QuickChange kit (Stratagene) using 50 ng of pASK-GabR construct as template and complementary oligonucleotides (GabR-R129Q-for and GabR-R129Q-rev; GabR-K362-366Q-for and GabR-K362-366Q-rev) harboring the mutation (Supplementary Table 1). Integrity of the constructs was verified by DNA sequencing. Expression and purification of the mutant proteins were performed as described for wild-type GabR.

2.2. Preparation of apo-GabR

Apo-GabR was prepared by incubating 100 µl of 140 µM holo-GabR with 100 µl of 200 mM L-cysteine at room temperature for 15 min [12]. Reaction of PLP with cysteine to form a thiazolidine adduct was monitored by absorbance changes in the wavelength range 260-600 nm. The protein was dialyzed overnight at 4 °C against storage buffer. Glycerol to a final concentration of 15% v/v was added and apo-GabR was stored at -80 °C.

2.3 Reduction of PLP Schiff bases with $NaBH_4$

The formation of the external aldimine between PLP and GABA was proven by reduction of the Schiff base with $NaBH_4$, following published methods [13]. A 85 µM solution of GabR was added of $NaBH_4$ to a final 7 mM concentration and incubated for about five min. The reaction, that can be followed spectrophotometrically, leads to the accumulation of a band at 335 nm that has been attributed to a substituted amine [14]. This treatment stabilizes the covalent bond between PLP and the amine that would otherwise undergo hydrolysis in solution after protein denaturation[15, 16]. After $NaBH_4$ treatment the sample was dialyzed overnight at 4 °C, against 6 M urea in 50 mM NaH_2PO_4 pH 8, 300 mM NaCl, 1 mM EDTA buffer. The solution was centrifuged and the absorption spectrum was recorded in the range 260-600 nm. GabR reduction was carried out in the absence and in the presence of 10 mM GABA. The retainment of the peak at 335 nm after denaturation and dialysis demonstrates that the reduction step involves a Schiff base between PLP and a protein residue. In the case of an external aldimine, i.e. a Schiff base with a substrate aminoacid, the substituted amine diffuses away during dialysis and no absorption at 335 nm is detected.

2.4. Spectroscopic measurements

Spectroscopic analyses were performed at room temperature using a Varian CARY400 spectrophotometer. The protein, at a concentration of 8 µM, was titrated with GABA (from 0 to 35 mM) in 100 mM HEPES pH 7.5, 100 mM NaCl. GABA dissociation constants of wild-type and mutant holo-GabR were determined by fitting the [GABA] dependence of the absorbance at 424 nm to a binding isotherm.

Far-UV CD spectra (260-195 nm) were collected using a JASCO J-715 spectropolarimeter. Measurements were performed at 25 ± 0.5 °C in 20 mM NaH_2PO_4 pH 7.5. Each spectrum is the average of three independent measurements and is subtracted of the buffer contribution.

2.5. Size exclusion chromatography

Gel filtration was performed on Ultrogel AcA44 resin (exclusion limit 200 kDa, operating range 17-175 kDa, column volume 63 ml and void volume 20.4 ml). Analysis of the GabR oligomerization state was carried out at 4 °C with 500 µl of 0.35 mg/ml GabR using a flow rate of 0.2 ml/min in 50 mM NaH_2PO_4 pH 8, 300 mM NaCl. The elution profiles were obtained by measuring the absorbance at 280 nm. The system was calibrated using the following molecular weight markers: aldolase (158 kDa), conalbumine (75 kDa), ovalbumin (44 kDa) and myoglobin (17 kDa). The void volume was defined by the elution volume of blue dextran (2000 kDa).

2.6. Cloning of wild-type and mutated gabTD promoters

The *gabTD* promoter region of *B. subtilis* strain WB800N was amplified by PCR from the position -244 to +169 with respect to the transcription start site of the *gabT* gene. The amplicon was digested with EcoRI and ligated to a linearized pNEB193 vector (New England BioLabs) with compatible ends to obtain the pNEB-gabTD construct. Mutant promoters used to characterize the GabR-DNA binding properties were obtained

by site-directed mutagenesis using primer extension for base insertion. Flanking primers, complementary to the ends of the target sequence and internal complementary primers, containing the mis-matched bases to insert or mutate, were used (Supplementary Table 1). First, two PCR reactions were assembled using one flanking primer and one internal primer. The amplicons of these PCRs were mixed and used as template for a third PCR reaction assembled with the flanking primers [17]. All constructs were obtained using the wt *gabTD* promoter except for pNEB-gabTDsub3 in which the pNEB-gabTDsub1 was used as template. The amplicon, containing the mutated sequence, was digested with EcoRI and ligated into a linearized pNEB193 vector with compatible ends. The 803, 808 and 813 bp long DNA fragments used in AFM experiments were obtained by PCR using Taq DNA polymerase and primers GabTD-800-for and GabTD-800-rev (Supplementary Table 1). All DNA fragments were gel purified and electroeluted using an Elutrap apparatus (Schleicher & Schuell, Keene, NH, USA). The recovered DNA was phenol/chloroform extracted, ethanol precipitated and resuspended in 5 mM Tris-HCl pH 8. The DNA concentration was determined by absorbance at 260 nm.

2.7. Construction of the MW vs volume calibration curve

The MW *vs* volume calibration curve used to infer the stoichiometry of the complexes, was obtained with five globular proteins of known MW: *Equus caballus* myoglobin (17 kDa), Bovine pancreas DNase I (30 kDa), Bovine serum albumin (66,5 kDa), Bovine liver catalase (250 kDa) and *Escherichia coli* RNA polymerase-ů70 (458 kDa). Each protein was diluted in deposition buffer (4 mM HEPES pH 7.4, 10 mM NaCl, 2 mM $MgCl_2$) at a concentration of 10-15 nM and deposited onto freshly-cleaved mica for 2 min. The mica disk was then rinsed with milliQ water and dryed with nitrogen. AFM images of 512×512 pixels were collected with a scan size of 1 µm at a scan rate of 2.5 lines per second. Volume of globular features was measured using the ñ*Zero basis*ò volume algorithm of the Gwyddion software (v2.38). Data were analyzed and graphed using SigmaPlot (SYSTAT Software, Inc.).

2.8. AFM of GabR-DNA complexes

Protein-DNA complexes were assembled using 20 nM DNA and 175 nM protein (holo-, apo- or mutant-GabR) in 10 mM HEPES pH 8, 50 mM KCl, 2 mM $MgCl_2$ and incubating the reaction at 25 °C for 15 min. When required, GabR was preincubated with 10 mM GABA at 25 °C for 15 min. prior to add the DNA. The reaction was diluted 10-fold in deposition buffer (4 mM HEPES pH 7.4, 10 mM NaCl, 2 mM $MgCl_2$) and 20 µl were deposited onto freshly-cleaved mica for 2 min. before the surface was rinsed with MilliQ water and dried with nitrogen. AFM imaging was carried out ñin airò with a Nanoscope IIIA microscope (Digital Instruments, Santa Barbara, CA, USA) equipped with the E scanner and commercial silicon cantilevers (MikroMasch, Tallinn, Estonia) operating in tapping mode. Images of 512×512 pixels were collected with a scan size of 2 µm at a scan rate of 2.5 lines per second.

2.9. Image analysis

DNA contour length measurements were performed as described in [18]using the following contour length estimator: L = (0.963ne + 1.362no) x S/W, where ñneò and ñnoò are the number of even and odd chain codes respectively, S is the image scan size, W is the image width in pixels. Position of the DNA bound GabR was manually selected by clicking the center of the protein with the mouse. The DNA contour length from the protein to the nearest end was defined short-arm while the DNA contour length from the protein to the farther end was defined long-arm. Complexes were classified as ñspecificò when the short arm/long arm ratio was of 0.65 ± 0.15. Outside this range of arm ratio the complexes were classified as ñnon-specificò.

The volume of GabR-DNA specific complexes was measured using Matlab (Mathworks, Natick, MA, USA). The complex boundaries were outlined with the free-hand tool and the mean height of the boundary pixels was used as reference background. The volume of the complex was computed by multiplying the surface area of the pixels within the boundary by their average pixel height relative to the reference background.

2.10. Dissociation constant determination from AFM images

To determine the dissociation constants of GabR-DNA complexes, we employed a previously developed methodology which requires knowledge of the fractional binding site occupancy, the average number of GabR dimers bound per DNA fragment and the total protein and total DNA concentrations of the reaction. Using the reverse of equation 5 in [19], *K*d can be expressed as:

$$K_d \approx \frac{(1 - O_{SP}) \times ([P] - [D] \times O_{Fragment})}{O_{SP}}$$

where: O_{SP} is the fractional binding site occupancy (the ratio between the number of specific complexes and the total number of DNA molecules in the pool of images); $O_{Fragment}$ is the average number of GabR dimers bound per DNA (this quantity is obtained by dividing the total number of complexes, specific and non-specific, by the total number of DNA molecules in the pool of images). [P] is the total GabR dimer concentration and [D] is the total DNA concentration. The term ([P] ï [D] × $O_{Fragment}$) represents the concentration of free GabR dimer. Thus, the determined *K*d will be referred to the GabR dimer. In each set of images, free and bound DNA molecules were manually counted. Specific and non-specific complexes were counted on the basis of their arm ratio.

2.11. Gel shift experiments

DNA mobility shift assays were conducted using purified GabR (from 6.3 to 400 nM dimer) and the *gabR-gabTD* intergenic region (10 nM). The intergenic region was amplified by PCR from the wild-type and mutant pNEB-gabTD plasmids using the oligonucleotides PgabRTD_for and PgabRTD_rev (Supplementary Table 1). The resulting 163-bp DNA fragments were incubated at 22 °C for 20 min in 10 µL of binding

buffer [20 mM HEPES, pH 8.0, containing 50 mM KCl, 5 mM $MgCl_2$, 1 mM DTT, 0.05% (v/v) NP-40, 30 μg/ml BSA and 5% (v/v) glycerol] with increasing concentrations of purified GabR. Where indicated, GABA and PLP were added to the final concentration of 20 mM and 1 μM, respectively, to ensure complete saturation. Samples were loaded onto 5% non-denaturing polyacrylamide gels in 0.5 x TBE buffer (45 mM Tris-borate, 1 mM EDTA). Gels were run at room temperature in 0.5 x TBE buffer and then incubated with SYBR Green (Sigma-Aldrich) for 10 min and visualized on a UV transilluminator.

2.12. Anomalous electrophoretic mobility for DNA bend angle determination

DNA fragments for bend angle determination by relative gel mobility were obtained by PCR from plasmid pNEB-gabTD, pNEB-gabTDins5 and pNEB-gabTDins10. Oligonucleotides GabRbsmiddle_for and GabRbsmiddle_rev (Supplementary Table 1) were used to obtain the 351 bp (wt), 356 bp (ins5) and 361 bp (ins10) DNA fragment with the GabR binding site in the middle, whereas oligonucleotides GabRbsend2_for and GabRbsend2_rev (Supplementary Table 1) were used to obtain the corresponding DNA fragment with the GabR binding site at one end. Primers were labelled with [γ-ATP-32P] (Perkin Elmer) using T4-polynucleotide kinase (Thermo Fisher Scientific). PCR was carried out in standard reaction conditions using Phusion DNA polymerase (Thermo Fisher Scientific). DNA fragments were purified with the molecular biology kit (Thermo Fisher Scientific) and DNA concentration was measured by NanoDrop ND-1000 (PeqLab). GabR- DNA complexes were assembled in 10 μl of binding buffer (10 mM HEPES pH 8, 50 mM KCl, 2 mM $MgCl_2$, 1 mM DTT, 30 μg/ml BSA and 5% glycerol) by mixing 10 fmol of 32P-labelled DNA with a 7X molar excess of wild-type GabR or 21X molar excess of GabR R129Q and GabR K362.366Q. The reaction was incubated at 25 °C for 15 min. Multiple A tract DNA fragments were obtained from restriction digestion of plasmids pJT170-2 through pJT170-8 [20] with NheI or BamHI and end-labelled with [γ-ATP-32P] using T4-polynucleotide kinase.

Electrophoresis was performed on a 6% polyacrylamide (37.5:1 acrylamide:bisacrylamide) gel in 0.5x TBE buffer (15x20 cm gel plates). Gels were run in cold room at 160 V for thirteen hours, dried and subjected to autoradiography using a Packard Cyclone (Alliance Analytical). Bend angle values are given as mean and SD of values determined from at least three independent experiments.

2.13. Prediction of DNA topology from sequence

The 3D structures of DNA of *gabTD wild-type*, *gabTDins5* and *gabTDins10* were determined with the Christoph Gohlke DNA Curvature Analysis service (http://www.lfd.uci.edu/~gohlke/dnacurve/) using the Bolshoi & Trifonov model [21]. A sequence of 253 bp, with the GabR binding site in the middle, was used in all cases.

2.14. Computation of electrostatic potential map

The PDB2PQR server (http://nbcr-222.ucsd.edu/pdb2pqr_2.0.0/) was used to compute the PQR file from the protein structure coordinates (PDB id: 4N0B). AMBER force field and PROPKA were used to calculate the

electrostatic potential at pH 8. The electrostatic potential map was mapped on the protein structure with the PyMOL Plugin APBS 2.1.

2.15. GabR-DNA docking

Docking protocol consists of rigid-body docking, semi-flexible refinement stage and final refinement in explicit solvent. Docking simulations were carried out using the GabR crystallographic structure (PDB id: 4N0B) and a 96 bp bent DNA fragment generated using the 3D-DART server (http://haddock.chem.uu.nl/dna) [22]. The DNA sequence corresponded to that from positions -60 to +36 of the *gabTD* promoter with a global DNA bending of 90° uniformly distributed between the two ATACCA direct repeats. GabR and DNA were docked using the data-driven docking program HADDOCK 2.1 [23]. Docking was performed by defining R43, S52 and K75 of each GabR monomer as ñactive residuesò interacting with 5ô-ATACCA direct repeats.

3. Results

3.1. Spectroscopic properties of GabR and reactivity with amino acids and GABA

The UV-visible absorption spectrum of holo-GabR (Figure 1) displays peaks at 340 nm and 425 nm. The peak at 425 is slightly red-shifted with respect to the peak of model Schiff bases, usually centered at about 415 nm [24]. However, most ATs show a peak centered between 410 and 435 nm, with aspartate AT showing a peak centered at 430 nm [25] and GABA AT at 415 nm [26, 27], representative of a protonated internal Schiff base formed between the catalytic lysine side chain and PLP. The peak at 340 nm could be the enolimine tautomer of the internal aldimine in equilibrium with the ketoenamine tautomer, or, as previously reported for other ATs, an unreactive PLP species [24]. After reduction with sodium borohydride ($NaBH_4$) followed by dialysis in 6 M urea, GabR displays an absorption spectrum with a peak at 330 nm. A control experiment omitting the reduction step was also carried out (Supplementary Figure S1A). This indicates that in the native protein PLP forms a Schiff base with a lysine residue that is reduced to a substituted amine by $NaBH_4$ as previously reported [14]. Differently from the unreduced GabR, this adduct is not released upon dialysis.

Addition of GABA to holo-GabR caused a decrease in the absorption at 425 nm and an increase at 340 nm (Figure 1). By fitting the dependence of the absorbance at 424 nm on GABA concentration to a binding isotherm equation, a *K*d of 1.98 ± 0.20 mM was determined, in agreement with other published data [5].

Previous spectroscopic studies of external aldimine formation in ATs, showed an increase of absorption at 430 nm instead of a decrease [28]. To test the hypothesis that GABA forms an external aldimine with PLP, GabR was subjected to $NaBH_4$ reduction in the presence of a saturating concentration of GABA (10 mM). Under these conditions, a band centered at 335 nm accumulates (Figure 1), similar to that obtained for the reduction of the internal aldimine (Supplementary Figure S1A). Overnight dialysis in 6 M urea led to the almost total loss of the reduced species, confirming the formation of the PLP external aldimine. A shoulder at 335 nm in the spectrum after dialysis (Figure 1), indicates that a small fraction of PLP does not react with GABA, as previously reported for PLP-dependent enzymes [13].

It has been demonstrated that GabR reacts with GABA but not with lysine, ornithine, asparagine, glutamine [5] and glycine up to 52 mM (Supplementary Figure S1A). Moreover, GabR reacts with cysteine to give a thiazolidine adduct [29] that can be removed from the active site of the protein by dialysis, to yield the apo-form of GabR (see Materials and Methods). Apo-GabR does not show any absorption peak in the visible region of the spectrum (Supplementary Figure S1A) and retains the secondary structure of the holo form, as shown by the far-UV circular dichroism spectra (Supplementary Figure S1B).

3.2. Investigation of protein-DNA complex formation using AFM

AFM was employed to investigate the interaction between GabR and the *gabTD* promoter. GabR-DNA complexes were assembled in 10 mM HEPES pH 8, 50 mM KCl and 2 mM $MgCl_2$ under different conditions and deposited onto freshly-cleaved mica as described in Material and Methods. A linear 803 bp DNA

fragment, with the GabR binding site located near the center, was used as template (Figure 2A). DNA fragments of this length make a strong interaction with the mica surface providing good sample deposition but at the same time they are short enough to allow 2D equilibration of the molecules onto the substrate [30]. Figure 2B depicts a 3D view of a typical AFM image of GabR-DNA complexes in which many of the DNA fragments have a protein bound in the position corresponding to the GabR cognate site. Because adhesion of the complexes to the hydrophilic mica surface may promote complex dissociation, GabR-DNA complexes were also analyzed after glutaraldehyde crosslinking. Under these conditions, no significant differences, neither in the number of complexes nor in their shape, were observed relative to uncrosslinked complexes (data not shown). Thus, all subsequent AFM analysis of GabR-DNA complexes was carried out without glutaraldehyde crosslinking.

AFM is a topographic technique [31, 32], so information regarding the stoichiometry of a nucleo-protein complex can readily be obtained from the volume of the protein particles bound to DNA [33-35]. However, because the scanning tip alters both the height and the width of protein complexes (by compression and by the tip-broadening effect), several authors have used calibration curves obtained with proteins of known molecular weight to infer the stoichiometry of the complexes [33]. Following this approach, a volume versus molecular weight (MW) plot was constructed using five globular proteins with a MW ranging from 17 to 458 kDa (Supplementary Figure S2). With the aim to reveal variation of the oligomerization state of GabR and/or the shape of the complexes, geometric parameters, such as the height, perimeter, surface area and volume of specific complexes were measured from the AFM images, as shown in Figure 2C,D and described in the Materials and Methods. The distribution of these measurements is shown in Figure 2E-H and the values are reported in Table 1. In particular, the distribution of volumes of GabR-DNA complexes has a mean of 260 ± 68 nm^3 which, on the basis of the Volume/MW calibration curve, corresponds to a complex of 120 kDa. This value is in good agreement with the MW of a GabR dimer (112 kDa), also considering that the protein-bound DNA can enlarge the volume of the complexes. Very similar results were also obtained with apo-GabR (Table 1), suggesting that PLP does not affect the binding stoichiometry of GabR. These results, together with the observed elution profile of GabR (Supplementary Figure S3), indicate that GabR binds the *gabTD* promoter as a dimer.

It has been shown that single molecule visualization by AFM can also be employed to assess the stability of the complexes by providing a direct way to determine the binding constant of nucleo-protein complexes under different conditions [19, 36]. To this end, we employed a previously developed statistical analysis of AFM images for the determination of protein-DNA site-specific binding constants (see Materials and Methods for details). The analysis relies on counting the different molecular species (DNA molecules, specific and non-specific complexes) scored within a large set of images of a binding reaction assembled with known protein and DNA concentrations. From these quantities we determined a statistically meaningful value for the DNA binding site occupancy under different conditions. The DNA binding site occupancy ' defined as the percent ratio between the number of complexes with GabR specifically bound at the *gabTD* promoter and the total number of DNA molecules (bound and unbound) ' was then used to determine the

microscopic dissociation constant of the protein-DNA complex. AFM images of complexes formed with holo- and apo-GabR at the wt *gabTD* promoter, show a similar number of complexes (Figure 3A,C) suggesting that PLP does not affect the DNA binding affinity of GabR. From the analysis of more than seventy images, we determined a *K*d of 10 ± 1 nM and 11 ± 1 nM for holo- and apo-GabR, respectively (Table 1). These values are supported by EMSA experiments conducted under similar conditions, except for the DNA fragment that was 163 bp long (Figure 3B,D).

3.3. Effect of GABA on the DNA binding properties

Expression of the *gabTD* operon is tightly connected to the transcription regulator activity of GabR. *In vitro* transcription assays demonstrated that in the presence of GABA, GabR activates the expression of the *gabT* and *gabD* genes [5, 6]. To get further insights on the role of the effector GABA, we evaluated the stoichiometry, affinity and structural features of holo-GabR-DNA complexes in the presence of saturating concentrations of GABA. AFM images of complexes formed with holo-GabR show a clear reduction of the number of complexes with an occupancy of 20.2 ± 0.7%, corresponding to a *K*d of 24 ± 1 nM, twice that measured in the absence of GABA (Figure 3E and Table 1). The effect of GABA on the DNA binding affinity of holo-GabR was also confirmed by EMSA (Figure 3F). In order to demonstrate that the effect of GABA on the DNA binding affinity of GabR is specifically determined by its binding into the GabR active site, we performed experiments with holo-GabR in the presence of 10 mM glycine which does not form an external aldimine with PLP (Supplementary Figure 1A). Under these conditions we determined a *K*d of 14 ± 2 nM, suggesting that the effect of GABA is due to a specific binding into the GabR active site with the formation of an external aldimine.

A change of the *K*d by a factor of two is not sufficient to justify the transcription activation of the *gabTD* promoter observed in the presence of GABA by a simple derepression mechanism. Literature data also indicate a small effect of GABA on the DNA binding affinity of GabR [5-7]. Nevertheless, binding of GABA to GabR could favor conformational changes of the protein that promote transcription initiation. Therefore, we carried out a detailed morphological analysis of the shape of the nucleo-protein complexes with the aim to reveal GABA-induced structural alterations. First, we measured geometrical parameters such as the height, perimeter and surface area and volume of complexes assembled in the presence and in the absence of GABA. As reported in Table 1, we determined an average volume value of 260 ± 68 nm^3 and 284 ± 77 nm^3, for holo- and apo-GabR, respectively. These values are very similar to those obtained with holo-GabR in the presence of GABA (276 ± 83 nm^3), further confirming that GabR binds the *gabTD* promoter as a dimer and indicating that GABA does not change the stoichiometry of the DNA-bound protein. However, we observed a decrease of the height of the complexes in the presence of GABA (from 1.7 ± 0.4 nm to 1.5 ± 0.4 nm; $P < 0.01$), with a concomitant increase of the perimeter (from 53 ± 7 nm to 59 ± 8 nm; $P < 0.01$) and surface area (from 275 ± 56 nm^2 to 324 ± 67 nm^2; $P < 0.01$) (see also Table 1). Furthermore, the DNA contour length analysis of the complexes reveals that binding of GabR to DNA determines a DNA

compaction of about 5 nm (the DNA contour length of free DNA is 258.8 ± 1.1 nm while that of GabR-DNA complexes is 253.7 ± 0.6 nm, mean and SD of three independent experiments; $P < 0.01$). It has been shown by us and by others that DNA onto mica can slightly reduce its contour length due to a partial transition from B- to A-form [37, 38]; to take this effect into account and to reduce experimental variability, the contour length of free DNA and GabR-DNA complexes was measured from the same set of images.

DNA compaction has been often ascribed to wrapping of DNA around the bound protein [39, 40], thus, the 5 nm DNA compaction observed for GabR is most probably due to the tight binding of the protein to an extended sequence of DNA. Interestingly, in the presence of GABA we did not observe such DNA compaction as the DNA contour length of the complexes remains of 260.4 ± 1.1 nm (mean and SD of two independent experiments), very similar to that of free DNA. Taken together these results suggest that GABA decreases the stability of the GabR-DNA complex and changes its conformation in a way that, under the AFM microscope, it appears less compacted.

3.4. DNA bend angle determination

It has been proposed that GabR can induce DNA deformation upon binding [7]. To assess whether GabR induces DNA bending, we employed polyacrylamide gel electrophoresis to detect and quantify anomalous mobilities of protein-DNA complexes formed either in the middle (μ_M) or at the end (μ_E) of linear DNA fragments. This gel shift assay is based on the assumption that a reduced end to end distance of the DNA fragment caused by the presence of a static bending, leads to a reduction in gel mobility. The relative mobility of the complexes was then used to estimate the DNA bend angle either by using the semiempirical equation proposed by Thompson and Landy [20]:

$$\mu_M/\mu_E = \cos(\alpha/2) \qquad \text{(eq. 1)}$$

where α is the DNA bending angle, or by using a set of DNA fragments harboring multiple phased A-tracts, as bending angle markers. As shown in Figure 3G, middle-bound holo-GabR complexes (lane 3) are retarded with respect to end-bound holo-GabR complexes (lane 4), indicating the presence of a significant DNA deformation. To support this interpretation and to infer the DNA bending angle, we used a set of linear DNA fragments ~350 bp long containing from two to eight phased A-tracts positioned either in the middle or near the end of the fragment. From the mobility ratio (μ_M/μ_E) we determined a bend angle of 81.6 ± 1.7 degrees using eq. 1 and a bend angle of 73.8 ± 1.8 degrees by using the calibration curve shown in Supplementary Figure S2C. Very similar DNA bending angles were obtained in the presence of 10 mM GABA (lanes 5 and 6, 79.4 ± 2.9 degrees using eq. 1 and 71.7 ± 3.4 degrees using the calibration curve) and with apoGabR (lanes 7 and 8, 79.0 ± 3.8 degrees using eq. 1 and 71.3 ± 4.6 degrees using the calibration curve). Although AFM has been used to measure protein induced DNA bending, such measurements result in very broad bend angle distributions (data not shown) probably because of the different orientation with which the complexes

stick to the mica surface. However, in the collected images we found several complexes with a shape compatible with a bend angle of 70-80° (Figure 3H).

3.5. Role of direct and inverted DNA sequence repeats in GabR binding

Published data indicate that GabR binds the *gabTD* promoter via two direct repeat hexamers (ATACCA) located upstream of the *gabTD* operon [6]. However, the crystallographic structure of GabR reveals that the protein is a domain-swap homodimer [4], a symmetry that in a wide number of cases preferentially recognizes inverted (palindromic) repeats rather than direct repeats [41]. Therefore, we focused on the *gabTD* promoter sequence to look for alternative DNA binding sequences that could account for this protein symmetry. Analysis of the *gabR-gabTD* interpromoter region of different *Bacillus* species showed that, beside the conserved ATACCA direct repeats, the intervening TGGTAC sequence, which has an inverted orientation with respect to ATACCA, is also conserved (Figure 4A). In order to evaluate the possible role of this inverted repeat in the GabR-*gabTD* promoter interaction, we constructed four promoter variants in which either the direct repeats or the identified inverted repeat were mutated (Figure 4B). Notice that in all mutants the length of the spacer between the two direct repeats was maintained constant. Next, GabR-DNA complexes assembled with these mutated promoters were analyzed by AFM and EMSA (Figure 4B and Table 1). With the *gabTDsub1* mutant, lacking the TGGTAC inverted repeat, we determined a microscopic *K*d of 13 ± 1 nM, very similar to that observed with the wild-type promoter. Likewise, with the *gabTDsub2* mutant, in which the downstream direct repeat was mutated, we obtained a *K*d of 35 ± 1 nM, thus suggesting that, although with some loss of affinity, GabR can still bind efficiently to the cognate site. Conversely, the simultaneous deletion of the downstream direct repeat and of the inverted sequence (*gabTDsub3*), resulted in a *K*d of 95 ± 8 nM, a value ten-fold higher than that of the wild-type promoter. These results were confirmed by EMSA experiments performed with the same set of mutants (Figure 4B, rows 1-3). Notably, the sole deletion of the upstream direct repeat (*gabTDsub4*) completely abolished GabR binding (Figure 4B, last row). The paucity of complexes formed with this promoter mutant did not permit to perform a statistically significant AFM analysis. Furthermore, the GabR binding affinity of the mutated promoters was also measured in the presence of a saturating concentration of GABA (Table 1 and Supplementary Figure S4). Under these conditions, for each mutant we observed an increase of the *K*d of about two-fold, in line with the effect of GABA observed with the wild-type promoter. These results indicate that binding of GabR to the *gabTD* promoter spans a DNA region beyond the previously identified direct repeats and highlight a possible specific interaction of GabR with the 29 bp DNA spacer separating the two ATACCA direct repeats.

3.6. Topology of the gabTD DNA affects the interaction with GabR

The *gabTD* promoter is characterized by an A/T-rich sequence, particularly in the spacer between the direct repeats, where 22 out of 29 bp are A or T. DNA fragments with a high A/T content often display DNA bending and a narrow minor groove [42, 43]. We investigated the relevance of the *gabTD* promoter topology in GabR binding, by first predicting the tridimensional structure of the *gabTD* promoter using the ñChristoph

Gohlke DNA curvature analysisò software (see Materials and Methods). As shown in Figure 5A (top row), the predicted structure of the 253 bp DNA harboring wt *gabTD* promoter displays a pronounced curvature.

To evaluate the role of DNA bending in the GabR-DNA binding mechanism, we constructed two *gabTD* mutants, one with an insertion of 5 bp (*gabTDIns5*) and the other with an insertion of 10 bp (*gabTDins10*) in the spacer region. Insertion of 5 bp determines a rotation of the DNA helix by half-turn, thus altering the DNA curvature (Figure 5A, middle row) and the phase of the direct and inverted repeats which are moved on the opposite side of the double helix. On the contrary, a 10 bp insertion increases the length of the spacer but should have a small effect on the overall curvature of the promoter and on the phase of specific binding sites (Figure 5A, bottom row).

Next, we analyzed the DNA binding properties of GabR to each one of the mutant promoters by EMSA and AFM (Figure 5B and 5C, respectively, and Table 1). With the *gabTDins5* mutant we observed a significant reduction of the number of specific complexes (occupancy only 4.8%) with a calculated *K*d of 72 ± 3 nM. The increased *K*d was confirmed by EMSA experiments showing that with this template only a slight band-shift is observed at high GabR concentration (Figure 5B, left gel). Conversely, the binding affinity of GabR for the *gabTDins10* mutant was only slightly affected, as indicated by the promoter occupancy of 31.8% and by the calculated *K*d of 12 ± 1 nM (Table 1). This result was also confirmed by EMSA (Figure 5B, right gel). By anomalous electrophoretic mobility we determined a bend angle of 71.4 ± 6.7 degrees for the GabR-*gabTDins10* complex and a bend angle of 65.1 ± 4.3 degrees for the GabR-*gabTDins5* complex (data not shown).

Visual inspection and measurement of the geometric properties of specific complexes formed with the *gabTDins10* mutant show interesting behaviors: first of all, the globular features representing the complexes, although formed in the expected position along the DNA template, appear blurred and not so well compacted as those observed with the wild-type template (Figure 5C). Secondly, the average height of the complexes is about 0.5 nm lower than that measured with the wild-type template (1.2 ± 0.3 nm against 1.7 ± 0.4 nm; $P < 0.01$), while both the perimeter and surface area increase significantly (from 53 ± 7 nm to 62 ± 9 nm; $P < 0.01$; from 275 ± 56 nm^2 to 350 ± 72 nm^2; $P < 0.01$;) (see also Table 1). On the other hand, the average volume of the complexes remains unchanged (260 ± 68 nm^3 against 253 ± 56 nm^3; $P > 0.016$), confirming the dimeric state of bound GabR. These results indicate that the curvature of the promoter DNA and the correct phasing of the two direct repeats are relevant features of the GabR-DNA interaction. They further suggest that GabR can accommodate a 10 bp (3.4 nm) lengthening of the spacer between the two direct repeats without a significant loss of affinity.

3.7. The AT domain of GabR displays a positively charged surface groove involved in DNA binding

Having found that the DNA spacer sequence is involved in the binding of GabR and that the DNA curvature or its bendability is a key determinant of the binding, we reasoned that there must also be protein residues specifically interacting with the promoter DNA beside those of the wHTH motif of the N-terminal domains. Analysis of the GabR surface electrostatic distribution shows the presence of a positively charged groove

running across the entire AT-fold domain (Figure 6A). This particular arrangement of basic amino acids (mainly lysines) is not observed in functional AT enzymes homologous of the GabR C-terminal domain (Figure 6B).

To get insights into the role played by the positively charged amino acids in GabR-DNA interaction, we employed site specific mutagenesis to construct GabR mutants with an altered positively charged surface. From the sequence alignment of GabR with several MocR members (Supplementary Figure S5), we have identified residues R129, K362 and K366 which are conserved among MocRs but not in AT enzymes. Therefore, GabR mutants R129Q and K362.366Q were constructed. Because GabR binds DNA as a homodimer, the positive groove of the two mutants loses two and four basic amino acids, respectively. The surface electrostatic potential of these mutants is shown in Figure 6C,D.

Before analyzing the DNA binding properties, these two GabR mutants were subjected to a biochemical and structural characterization. In particular, the UV-visible absorption spectra of mutant GabR were identical to that of the wild-type protein, with the internal aldimine peaks at 340 and 425 nm (Figure 7A). The far-UV circular dichroism spectra did not show significant differences in the secondary structure between mutated and wild-type GabR (Figure 7B). Likewise, thermal denaturation curves showed similar behaviors between mutated and wild-type GabR (Supplementary Figure S6). AFM volume measurements of mutant protein particles were very similar to those obtained with the wild-type GabR, suggesting that the mutations do not affect the oligomerization state of the protein (data not shown). Titration with GABA, in the concentration range from 0 to 35 mM, determined a decrease of the absorption at 425 nm and an increase of the absorption at 340 nm, indicating the formation of an external aldimine. Estimated GabR-GABA *K*d values were 2.67 ± 0.68 mM and 1.40 ± 0.10 mM for the R129Q and K362.366Q mutants, respectively (Figure 7C,D), to be compared with the *K*d of 1.98 ± 0.20 mM determined for wild-type GabR.

Next, we measured the DNA-binding properties of GabR mutants with the wt *gabTD* promoter. The GabR R129Q mutant displays a *K*d of 22 ± 1 nM, twice that of wild-type GabR. This value was also confirmed by EMSA assay (Figure 7E). Thus, this mutation affected the GabR binding affinity only slightly. Conversely, the GabR K362.366Q mutant showed a dramatically reduced binding affinity with a *K*d of 252 ± 31 nM. EMSA experiments show that this mutant does not shift the promoter DNA electrophoretic mobility at all the concentrations tested (Figure 7F). From the anomalous electrophoretic mobility of the R129Q mutant we determined a bend angle of 81.7 ± 1.3 degrees using eq. 1 and a bend angle of 73.9 ± 1.4 degrees by using the calibration curve. No binding was observed with the K362.366Q mutant (Figure 7G).

Moreover, as shown in Table 1, the geometric parameters of the complexes assembled with the GabR R129Q suggest that the complexes have a larger perimeter (from 53 ± 7 nm to 65 ± 10 nm; $P < 0.01$;) and surface area (from 275 ± 56 nm^2 to 390 ± 96 nm^2; $P < 0.01$;) and a smaller height (from 1.7 ± 0.4 nm to 1.3 ± 0.5 nm; $P < 0.01$;) than those obtained with wild-type GabR. Similar results were obtained with GabR K362.366Q mutant. As outlined above for the *gabTD* promoter mutants, these variations represent a direct evidence of an altered protein-DNA interaction.

These results demonstrate that the substitution of two lysine residues in the AT-fold domain impairs the binding of GabR to the *gabTD* promoter DNA, or at least dramatically affects the energetics of binding, and suggest that the positively charged groove on the surface of GabR plays an important role in the interaction with DNA.

3.8. Structural model of the GabR-DNA interaction

Published data, in conjunction with the structural information obtained in this study, were used to guide a GabR-*gabTD* docking simulation using the HADDOCK server [23]. To date no structural information is available for the GabR-DNA complex, thus to identify putative DNA binding residues of GabR, Edayathumangalam and colleagues investigated *E. coli* FadR because its HTH DNA-binding domain is homologous to that of GabR and because the crystal structure of the FadR-DNA complex is available [4]. Moreover, FadR binds TCTGGT inverted repeat hexamers [44], complementary to the direct repeats recognized by GabR (ATACCA). Simulation of the interaction between one copy of the GabR wHTH domain and the sequence recognized by FadR provided an identical binding architecture to that observed in FadR-DNA crystal structure [4]. This observation suggests that GabR residues, R43, S52 and K75, are good candidates for the specific recognition of the ATACCA direct repeats. In particular, GabR R43 could interact with one of the guanines in the direct repeat [4].

Because there are evidences that GabR binds DNA as a dimer and that the topology of the promoter DNA is an important determinant of the specific recognition, we performed the docking simulation using a GabR dimer and a DNA fragment harboring the *gabTD* promoter region with an intrinsic curvature of 80° (as estimated by anomalous electrophoretic mobility) evenly distributed between the two direct repeats. Notably, docking simulations performed using a straight DNA fragment or a DNA with intrinsic bending as predicted from the sequence by the Bolshoi-Trifonov model [21], did not converge. Docking simulations performed using a DNA fragment with a bend larger than 90° resulted in loss of contact between the DNA and the protein. Figure 8 shows the docking simulation with the best score (cluster 6, score parameters reported in the Supplementary Table 2), obtained by defining residue R43 as ñactive residueò interacting with the ATACCA direct repeat hexamer. As expected, the DNA spacer region bends against the protein surface making an extended contact that involves the two wHTH domains and the intervening surface of the AT domains of the dimer, incidentally where the positive groove is mapped. The Ŭ2 helix of the wHTH motif invades the major groove to specifically recognize one guanine of the hexamer, while residues of the Ŭ3 interact with the phosphate backbone. On the contrary, the orientation of the other wHTH domain is not ideal to perform the same interaction with the second direct repeat sequence. However, during the GabR-DNA complex assembly, it is possible that the long and flexible linker that connects the wHTH domain to the AT-fold domain promotes tridimensional rearrangements necessary to correctly interact with the direct repeat sequence. Importantly, this model suggests that GabR residue R129 makes contacts with the GC base pair of the inverted sequence while several hydrogen bonds can be formed between residues K125, K133, K362,

K365, K366 and DNA phosphates (Figure 8D). It should be pointed out that none of the AT domain residues was defined as ñactive residueò in the docking simulation.

4. Discussion

The strep-tagged holo-GabR shows spectroscopic properties similar to those already described for a different GabR construct [5] and reacts with GABA with the accumulation of the external aldimine. Since an increase in the peak at 340 nm is *per se* not indicative of external aldimine formation, we employed $NaBH_4$ reduction, followed by dialysis under denaturing conditions, to assess whether the PLP-GABA adduct is still bound to the protein active site. Under these conditions, most of the PLP dissociates from the protein, indicating that a large fraction of PLP has reacted with GABA to form an external aldimine (Figure 1) [4, 5]. Notably, the enolimine tautomer of PLP Schiff base, that is favored over the ketoenamine in less polar environments [45], is more populated in the external than in the internal aldimine (Figure 1), suggesting that binding of GABA induces a conformational change of GabR affecting (also) the polarity of PLP binding site. The R129Q and K362.366Q mutations do not lead to any appreciable change in GabR affinity for GABA (Figure 7C-D). This finding, together with no appreciable influence of mutations on the protein secondary structure (Figure 7B), indicates that the mutations do not perturb the protein overall fold and its ability to correctly bind and react with GABA.

Despite there is no crystal structure available of the GabR-DNA complex, different models have been proposed to describe the binding architecture and the possible mode of action of this regulator [4]. Recent evidences suggest that GabR binds DNA as a dimer by an interaction of the wHTH motif of the N-terminal domains with direct repeats found in the upstream region of the *gabTD* promoter [5, 7]. Our AFM analysis shows that the volume of GabR-DNA complexes is compatible with a binding stoichiometry of one GabR dimer per cognate site. The data also exclude the possibility that a tetramer could bind the two direct repeats.

By using a previously developed AFM methodology to determine protein-DNA complex stability [19], we were able to estimate the dissociation constant of GabR-DNA complexes under different conditions. Comparison of the DNA binding properties of holo- and apo-GabR indicates that the two forms of the protein have a similarly high affinity for the *gabTD* promoter (*K*d of 10 nM for both forms), suggesting that the PLP is not required to support GabR-DNA binding. A similar result was also obtained with *Rhodobacter capsulatus* TauR, which binds to the *tpa* promoter independently of the presence of PLP and its effector taurine [9]. Interestingly, a 2.4 fold increase of the *K*d was observed in the presence of GABA but not in the presence of glycine, suggesting that the destabilizing effect must arise from protein conformational changes triggered by the binding of GABA. Although GABA destabilizes the GabR-DNA complex, simple promoter disclosure does not seems to be the main action mechanism of *gabTD* control, as the *K*d remains in the nM regime. *In vitro* transcription experiments demonstrated that PLP and GABA are required for *gabTD* activation [5, 6], supporting the hypothesis that GABA may induce structural rearrangements of GabR that

could activate transcription initiation by recruiting the RNAP or by favoring the transition from closed to open complex. The change in height and perimeter of the complexes revealed by AFM in the presence of GABA, together with the change of the DNA contour length (Table 1), may be a direct evidence of this conformational change. Remarkably, a conformational change of GabR in the presence of GABA has also been proposed based on the increase of the radius of gyration of the protein determined by SAXS [7], and is consistent with the change in the relative population of enolimine and ketoenamine tautomers of PLP that we report for holo-GabR (Figure 1).

The specific interaction between a protein and DNA relies on both ñdirectò protein-nucleotide contacts and ñindirectò recognition of the sequence-dependent tridimensional shape of the DNA. For dimeric proteins that recognize direct or inverted repeats, the length, curvature and flexibility of the intervening sequence also play a key role in the interaction because they control the correct positioning of base atoms with respect to amino acid residues. It has recently been proposed that the DNA shape of the *gabTD* promoter region is an important determinant of the complex formation and stability [7]. Accordingly, the high A/T content of the GabR DNA binding region suggests that the *gabTD* promoter may display some degree of intrinsic bending as predicted by the Bolshoi-Trifonov model [21]. Our anomalous electrophoretic mobility assays show that upon binding, GabR bends the cognate site DNA by 70-80° (Figure 3). Such a large DNA bending is consistent with the binding of the wHTH domains to the ATACCA direct repeats and with an extended interaction between the intervening sequence and GabR AT domains. Insertion of 5 bp in between the binding sites, which due to the DNA helical twist (10.5 bp/turn) not only moves the sites ~1.7 nm apart but also rotates their major groove on opposite sides of the DNA double helix, affects both the GabR binding affinity (*K*d = 72 ± 3 nM) and conformation of the complexes (bend angle 65°). On the other hand, a 10 bp insertion affects GabR binding only slightly (*K*d = 12 ± 1 nM) and has little effect on bending (bend angle 71°), suggesting that the correct phasing of the direct repeats is crucial for binding, and that GabR can accommodate an increased distance between the direct repeats if the phase of the DNA double helix is maintained. The long and flexible linkers connecting the wHTH domains to the AT domains may be accountable for this protein plasticity.

Next, we focused our attention on the surface of the GabR AT domains that may be facing the DNA spacer between the two ATACCA. Differently from other homologous AT enzymes, several lysine residues form a longitudinal basic groove on the surface of GabR AT-domains (Figure 6). To evaluate the role of this positively charged surface in the interaction with DNA, we produced two GabR mutants, R129Q and K362.366Q, with reduced positive charge. R129Q displayed a slight reduction of the DNA binding affinity, leaving virtually unaffected the DNA bending angle (Figure 7). Conversely, binding was dramatically impaired for the double mutant K362.366Q, suggesting that the basic groove on the surface of the AT-domains is an important determinant of the DNA interaction. The relevance of this finding is supported by the conservation of the positively charged groove in other MocR members such as *B. clausii* PdxR, as predicted by structural homology modeling [10], which shares direct repeats recognition and probably the entire DNA binding architecture with GabR. Furthermore, a chimeric protein composed of the GabR wHTH

DNA binding domain and the *Thermus thermophilus* 2-aminoadipate aminotransferase domain, lacking the basic groove, showed a lower binding affinity for the *gabTD* promoter relative to wild-type GabR [46].

4.1. Proposed model of the GabR-gabTD interaction

Based on our findings and on published data, we generated a structural model by docking the crystal structure of GabR with the 96 bp DNA sequence of the binding site using the HADDOCK docking server [23]. By providing either a straight DNA or a bent DNA as obtained with the Bolshoi-Trifonov model, docking failed, meaning that the program could not find a structure for the complex that could satisfy binding requirements of the wHTH with the ATACCA repeats. Docking was instead successful when using a bent DNA with an 80° curvature (as suggested by our anomalous electrophoretic mobility data) evenly distributed between the ATACCA repeats. The model also predicts that the bent DNA lies on the longitudinal groove of basic residues of the AT-fold domain. In particular, R129 specifically recognize a GC base pair of the inverted sequence in the DNA spacer, whereas K125, K133, K362, K365, K366 contact the phosphates of the DNA backbone. Deletion of this inverted repeat has little or no effect on GabR binding (*K*d = 13 ± 1 nM), in agreement with a previous mutational analysis [6]. Similarly, deletion of the sole downstream ATACCA direct repeat modestly increases the *K*d to 35 ± 1 nM. However, when the inverted repeat and downstream direct repeat were simultaneously deleted, binding was highly compromised (*K*d = 95 ± 8). Notably, deletion of the sole upstream direct repeat is sufficient to abolish binding as revealed by EMSA. The resulting picture is a complex pattern of interaction exploiting the specific recognition between the wHTH domains and the ATACCA direct repeats [4, 44], the curvature of the *gabTD* promoter region [7], the here proposed interaction of residues of the AT-fold domains with the inverted repeat and the electrostatic interaction between positively charged residues of the AT-fold domains and negatively charged DNA phosphates found at the protein-DNA interface. This extended electrostatic interaction may stabilize the highly bent DNA conformation through asymmetric phosphate neutralization [47], a mechanism that has been proposed for other DNA binding proteins [48].

Finally, GabR crystallographic data suggest that the orientation of the N-terminal domains is not ideal to accommodate the interaction with the two direct repeats. For this reason, it has been proposed that the weak interaction at the interface between the N-terminal domain and the AT-fold domain, together with the flexible and long linker, can promote the wHTH domain reorientation necessary to correctly house the direct repeats [7]. Although we do not exclude this hypothesis, our results raise the possibility that the interaction of the two wHTHs with the ATACCA direct repeats may not be symmetric, and the different affinity observed for *gabTDsub2* relative to *gabTDsub4* (Table 1) supports this hypothesis. Given the position of the *gabTD* -35 hexamer, this asymmetric binding mode of GabR could be part of the mechanism governing the switch between promoter repression and activation.

5. Funding

DA is supported by Chiesi Farmaceutici. TM is supported by Regione Lazio - ProTox project - Prot. FILAS-RU-2014 ï 1020. This work was partly supported by grants from the University of Parma [to C.R.] and from Finanziamento Progetto di Ricerca di Università 2014 (prot. C26A14SY4E) of Sapienza University of Rome [to M.L.dS.].

6. Acknowledgements

We would like to thank Prof. Andrea Mozzarelli for helpful discussion. We also thank the Centro Interdipartimentale Misure of the University of Parma for the AFM facility.

References

[1] B.R. Belitsky, A.L. Sonenshein, GabR, a member of a novel protein family, regulates the utilization of gamma-aminobutyrate in Bacillus subtilis, Mol Microbiol, 45 (2002) 569-583.

[2] S. Rigali, A. Derouaux, F. Giannotta, J. Dusart, Subdivision of the helix-turn-helix GntR family of bacterial regulators in the FadR, HutC, MocR, and YtrA subfamilies, J Biol Chem, 277 (2002) 12507-12515.

[3] E. Bramucci, T. Milano, S. Pascarella, Genomic distribution and heterogeneity of MocR-like transcriptional factors containing a domain belonging to the superfamily of the pyridoxal-5'-phosphate dependent enzymes of fold type I, Biochem Biophys Res Commun, 415 (2011) 88-93.

[4] R. Edayathumangalam, R. Wu, R. Garcia, Y. Wang, W. Wang, C.A. Kreinbring, A. Bach, J. Liao, T.A. Stone, T.C. Terwilliger, Q.Q. Hoang, B.R. Belitsky, G.A. Petsko, D. Ringe, D. Liu, Crystal structure of Bacillus subtilis GabR, an autorepressor and transcriptional activator of gabT, Proc Natl Acad Sci U S A, 110 (2013) 17820-17825.

[5] K. Okuda, S. Kato, T. Ito, S. Shiraki, Y. Kawase, M. Goto, S. Kawashima, H. Hemmi, H. Fukada, T. Yoshimura, Role of the aminotransferase domain in Bacillus subtilis GabR, a pyridoxal 5'-phosphate-dependent transcriptional regulator, Mol Microbiol, 95 (2015) 245-257.

[6] B.R. Belitsky, Bacillus subtilis GabR, a protein with DNA-binding and aminotransferase domains, is a PLP-dependent transcriptional regulator, J Mol Biol, 340 (2004) 655-664.

[7] W.A. Al-Zyoud, R.M. Hynson, L.A. Ganuelas, A.C. Coster, A.P. Duff, M.A. Baker, A.G. Stewart, E. Giannoulatou, J.W. Ho, K. Gaus, D. Liu, L.K. Lee, T. Bocking, Binding of transcription factor GabR to DNA requires recognition of DNA shape at a location distinct from its cognate binding site, Nucleic Acids Res, 44 (2016) 1411-1420.

[8] D. Jain, Allosteric control of transcription in GntR family of transcription regulators: A structural overview, IUBMB life, 67 (2015) 556-563.

[9] J. Wiethaus, B. Schubert, Y. Pfander, F. Narberhaus, B. Masepohl, The GntR-like regulator TauR activates expression of taurine utilization genes in Rhodobacter capsulatus, J Bacteriol, 190 (2008) 487-493.

[10] A. Tramonti, A. Fiascarelli, T. Milano, M.L. di Salvo, I. Nogues, S. Pascarella, R. Contestabile, Molecular mechanism of PdxR - a transcriptional activator involved in the regulation of vitamin B6 biosynthesis in the probiotic bacterium Bacillus clausii, The FEBS journal, 282 (2015) 2966-2984.

[11] A. Kalia, A. Rattan, P. Chopra, A method for extraction of high-quality and high-quantity genomic DNA generally applicable to pathogenic bacteria, Anal Biochem, 275 (1999) 1-5.

[12] K. Cai, D. Schirch, V. Schirch, The affinity of pyridoxal 5'-phosphate for folding intermediates of Escherichia coli serine hydroxymethyltransferase, J Biol Chem, 270 (1995) 19294-19299.

[13] D. Schiroli, L. Ronda, A. Peracchi, Kinetic characterization of the human O-phosphoethanolamine phospho-lyase reveals unconventional features of this specialized pyridoxal phosphate-dependent lyase, The FEBS journal, 282 (2015) 183-199.

[14] R.C. Hughes, W.T. Jenkins, E.H. Fischer, The site of binding of pyridoxal-5'-phosphate to heart glutamic-aspartic transaminase, Proc Natl Acad Sci U S A, 48 (1962) 1615-1618.

[15] E.H. Cordes, W.P. Jencks, On the Mechanism of Schiff Base Formation and Hydrolysis, Journal of the American Chemical Society, 84 (1962) 832-837.

[16] E.S. Simon, J. Allison, Determination of pyridoxal-5'-phosphate (PLP)-bonding sites in proteins: a peptide mass fingerprinting approach based on diagnostic tandem mass spectral features of PLP-modified peptides, Rapid Communications in Mass Spectrometry23 (2009) 3401-3408.

[17] J. Reikofski, B.Y. Tao, Polymerase chain reaction (PCR) techniques for site-directed mutagenesis, Biotechnology advances, 10 (1992) 535-547.

[18] C. Rivetti, A simple and optimized length estimator for digitized DNA contours, Cytometry A, 75 (2009) 854-861.

[19] Y. Yang, L.E. Sass, C. Du, P. Hsieh, D.A. Erie, Determination of protein-DNA binding constants and specificities from statistical analyses of single molecules: MutS-DNA interactions, Nucleic Acids Res, 33 (2005) 4322-4334.

[20] J.F. Thompson, A. Landy, Empirical estimation of protein-induced DNA bending angles: applications to lambda site-specific recombination complexes, Nucleic Acids Res, 16 (1988) 9687-9705.

[21] A. Bolshoy, P. McNamara, R.E. Harrington, E.N. Trifonov, Curved DNA without A-A: experimental estimation of all 16 DNA wedge angles, Proc Natl Acad Sci U S A, 88 (1991) 2312-2316.

[22] M. van Dijk, A.M. Bonvin, 3D-DART: a DNA structure modelling server, Nucleic Acids Res, 37 (2009) W235-239.

[23] M. van Dijk, A.D. van Dijk, V. Hsu, R. Boelens, A.M. Bonvin, Information-driven protein-DNA docking using HADDOCK: it is a matter of flexibility, Nucleic Acids Res, 34 (2006) 3317-3325.

[24] R. Kallen, T. Korpela, A. Martell, Y. Matsushima, C. Metzler, D. Metzler, Y. Morozov, I. Ralston, F. Savin, Y. Torchinsky, H. Ueno, Chemical and spectroscopic properties of pyridoxal and piridoxamine phosphates in: C. P., M. D.E. (Eds.) Transaminases, Wiley, New York, 1985, pp. 37–108.

[25] D.E. Metzler, Tautomerism in pyridoxal phosphate and in enzymatic catalysis, Advances in enzymology and related areas of molecular biology, 50 (1979) 1-40.

[26] P. Storici, D. De Biase, F. Bossa, S. Bruno, A. Mozzarelli, C. Peneff, R.B. Silverman, T. Schirmer, Structures of gamma-aminobutyric acid (GABA) aminotransferase, a pyridoxal 5'-phosphate, and [2Fe-2S] cluster-containing enzyme, complexed with gamma-ethynyl-GABA and with the antiepilepsy drug vigabatrin, J Biol Chem, 279 (2004) 363-373.

[27] K. Yonaha, K. Suzuki, S. Toyama, 4-Aminobutyrate:2-oxoglutarate aminotransferase of Streptomyces griseus: purification and properties, European journal of biochemistry / FEBS, 146 (1985) 101-106.

[28] M. Sterk, H. Gehring, Spectroscopic characterization of true enzyme-substrate intermediates of aspartate aminotransferase trapped at subzero temperatures, European journal of biochemistry / FEBS, 201 (1991) 703-707.

[29] M.V. Buell, R.E. Hansen, Reaction of Pyridoxal-5-phosphate with Aminothiols, Journal of the American Chemical Society, 82 (1960) 6042-6049.

[30] C. Rivetti, M. Guthold, C. Bustamante, Scanning force microscopy of DNA deposited onto mica: equilibration versus kinetic trapping studied by statistical polymer chain analysis, J Mol Biol, 264 (1996) 919-932.

[31] C. Bustamante, C. Rivetti, Visualizing protein-nucleic acid interactions on a large scale with the scanning force microscope, Annu Rev Biophys Biomol Struct, 25 (1996) 395-429.

[32] A. Alessandrini, P. Facci, AFM: a versatile tool in biophysics, Meas Sci Technol, 16 (2005) R65-R92.

[33] C. Wyman, E. Grotkopp, C. Bustamante, H.C.M. Nelson, Determination of heat-shock transcription factor 2 stoichiometry at looped DNA complexes using scanning force microscopy, EMBO J., 14 (1995) 117-123.

[34] P.N. Minh, N. Devroede, J. Massant, D. Maes, D. Charlier, Insights into the architecture and stoichiometry of Escherichia coli PepA*DNA complexes involved in transcriptional control and site-specific DNA recombination by atomic force microscopy, Nucleic Acids Res, 37 (2009) 1463-1476.

[35] Y.L. Li, Y.F. Meng, Z.M. Zhang, Y. Jiang, Detecting the oligomeric state of Escherichia coli MutS from its geometric architecture observed by an atomic force microscope at a single molecular level, The journal of physical chemistry. B, 118 (2014) 9218-9224.

[36] N. Doniselli, P. Rodriguez-Aliaga, D. Amidani, J.A. Bardales, C. Bustamante, D.G. Guerra, C. Rivetti, New insights into the regulatory mechanisms of ppGpp and DksA on Escherichia coli RNA polymerase-promoter complex, Nucleic Acids Res, 43 (2015) 5249-5262.

[37] C. Rivetti, S. Codeluppi, Accurate length determination of DNA molecules visualized by atomic force microscopy: evidence for a partial B- to A-form transition on mica, Ultramicroscopy, 87 (2001) 55-66.

[38] A. Japaridze, D. Vobornik, E. Lipiec, A. Cerreta, J. Szczerbinski, R. Zenobi, G. Dietler, Toward an Effective Control of DNA's Submolecular Conformation on a Surface, Macromolecules, 49 (2016) 643-652.

[39] C. Rivetti, M. Guthold, C. Bustamante, Wrapping of DNA around the E.coli RNA polymerase open promoter complex, Embo J, 18 (1999) 4464-4475.

[40] S. Maurer, J. Fritz, G. Muskhelishvili, A. Travers, RNA polymerase and an activator form discrete subcomplexes in a transcription initiation complex, Embo J, 25 (2006) 3784-3790.

[41] P.A. Rice, C.C. Correll, Protein-nucleic acid interactions : structural biology, RSC Pub., Cambridge, 2008.

[42] J. Hizver, H. Rozenberg, F. Frolow, D. Rabinovich, Z. Shakked, DNA bending by an adenine--thymine tract and its role in gene regulation, Proc Natl Acad Sci U S A, 98 (2001) 8490-8495.

[43] R. Rohs, S.M. West, A. Sosinsky, P. Liu, R.S. Mann, B. Honig, The role of DNA shape in protein-DNA recognition, Nature, 461 (2009) 1248-1253.

[44] Y. Xu, R.J. Heath, Z. Li, C.O. Rock, S.W. White, The FadR-DNA complex. Transcriptional control of fatty acid metabolism in Escherichia coli, J Biol Chem, 276 (2001) 17373-17379.

[45] E.J. Faeder, G.G. Hammes, Kinetic studies of tryptophan synthetase. Interaction of L-serine, indole, and tryptophan with the native enzyme, Biochemistry, 10 (1971) 1041-1045.

[46] K. Okuda, T. Ito, M. Goto, T. Takenaka, H. Hemmi, T. Yoshimura, Domain characterization of Bacillus subtilis GabR, a pyridoxal 5'-phosphate-dependent transcriptional regulator, Journal of biochemistry, 158 (2015) 225-234.

[47] A.D. Mirzabekov, A. Rich, Asymmetric lateral distribution of unshielded phosphate groups in nucleosomal DNA and its role in DNA bending, Proc Natl Acad Sci U S A, 76 (1979) 1118-1121.

[48] P.R. Hardwidge, J.M. Zimmerman, L.J. Maher, 3rd, Charge neutralization and DNA bending by the Escherichia coli catabolite activator protein, Nucleic Acids Res, 30 (2002) 1879-1885.

Figure legends

Figure 1. Absorption spectra of holo-GabR titrated with GABA in the range 0-35 mM (black lines). The absorbance decrease at 425 nm and increase at 340 nm indicates formation of an external aldimine with GABA. GabR saturated with GABA was reduced by addition of $NaBH_4$ (red line) and the spectrum recorded after O/N dialysis to remove unbound PLP (green line). Inset: dependence of the absorption at 425 nm on GABA concentration. Data are fitted to a binding isotherm with *K*d = 1.98 ± 0.20 mM.

Figure 2. A) Schematic representation of the DNA fragment harboring the *gabTD* promoter used in AFM experiments. Direct repeats recognized by GabR are in boxes. B) 3D-AFM image of holo-GabR in complex with the *gabTD* promoter. C) GabR-DNA complex outlined with the black mask used for perimeter, surface area and volume determination. D) Image profile along the dashed line drawn in C. E-H) Distributions of the geometric parameters measured on specific GabR-*gabTD* complexes. Values are reported in **Table 1**.

Figure 3. Effect of PLP and GABA on the binding of GabR to the *gabTD* promoter. A) AFM image of holo-GabR-DNA specific complexes (indicated by arrows) and corresponding polyacrylamide gel mobility-shift assay (B). C) AFM image of apo-GabR-DNA complexes and corresponding polyacrylamide gel mobility-shift assay (D). E) AFM image of holo-GabR-GABA/DNA complexes and corresponding polyacrylamide gel mobility-shift assay (F). In B, D and F protein concentration is reported as nM dimer. G) Anomalous electrophoretic mobility of GabR-DNA complexes formed with a 351 bp DNA fragment harboring the cognate site in the middle (lanes 1, 3, 5, 7) or at the end (lanes 2, 4, 6, 8). Lanes 1 and 2 free DNA; lanes 3 and 4 holo-GabR; lanes 5 and 6 holo-GabR-GABA; lanes 7 and 8 apo-GabR. H) Selected GabR-DNA complexes with a DNA bending consistent with the anomalous electrophoretic mobility data.

Figure 4. A) Alignment of the *gabTD* promoter region of six *Bacillus* species: *Bacillus subtilis* subsp. *subtilis* strain 168, *Bacillus subtilis* subsp. *spizizenii* TU-B-10, *Bacillus atrophaeus* subsp. *globigii*, *Bacillus amyloliquefaciens* DSM 7, *Bacillus licheniformis* DSM 13 (ATCC 14580), and *Halobacillus halophilus* DSM 2266. Arrows indicate the position and the orientation of the ATACCA direct repeats and the TGGTAC inverted sequence. Gray boxes indicate the -10 and -35 hexamers of the *gabTD* promoter. B) Schematic representation and DNA sequence of wild-type and mutant *gabTD* promoters. Direct repeats and inverted sequences are underlined and indicated by arrows. For each DNA template, the corresponding gel mobility-shift assay with holo-GabR is shown on the right. A DNA fragment of 163 bp was used in each experiment. GabR concentration is reported as nM dimer. Gels were stained with SYBR Green.

Figure 5. A) Schematic representation and DNA sequence of wild-type and mutant *gabTD* promoters (left). Arrows represent direct repeats; shaded arrow indicates opposite DNA face. Inserted DNA sequences are underlined and represented by boxes. Right: corresponding three-dimensional bending prediction of a 253 bp DNA sequence from position -166 to + 87 relative to the *gabT* +1. Dots indicate the position of direct repeats. B) Polyacrylamide gel mobility-shift assays of *gabTDIns5* and *gabTDIns10* promoter mutants with holo-GabR. A DNA fragment of 163 bp was used in each experiment as detailed in Materials and Methods. GabR concentration is reported as nM dimer. Gels were stained with SYBR Green. C) Gallery of specific holo-GabR-DNA complexes formed with the wt *gabTD* DNA fragment (left column) and with the *gabTDIns10* DNA fragment (right column). The image profile of each complex is shown on the right. Solid line: wt *gabTD*; dash line: *gabTDIns10*.

Figure 6. Electrostatic potential surface map of A) *B. subtilis* GabR (PDB ID 4N0B), B) *Thermus thermophilus* 2-aminoadipate aminotransferase (PDB ID 2EGY), C) in silico mutant GabR R129Q, D) in silico mutant GabR K362.366Q. The values ī 1.000 $kTe^{ī 1}$ and +1.000 $kTe^{ī 1}$ represent acidic (red) and basic (blue) potential surface charges, respectively.

Figure 7. Absorption (A) and circular dichroism (B) spectra of wild-type holo-GabR, GabR R129Q and GabR K362.366Q. The R129Q and K362.366Q mutant (panel C and D, respectively) were titrated with GABA at 25 °C in 100 mM HEPES pH 7.5, 100 mM NaCl. The insets in panels C and D report the corresponding change of the absorption at 425 nm as a function of [GABA] fitted to the equation for a binding isotherm (continuous lines) yielded a *K*d of 2.67 ± 0.68 mM and 1.40 ± 0.10 mM for the R129Q and K362.366Q mutants, respectively. E) Polyacrylamide gel mobility-shift assays of a wt *gabTD* DNA fragment with GabR R129Q. F) Polyacrylamide gel mobility-shift assays of a wt *gabTD* DNA fragment with GabR K362.366Q. Protein concentration is reported as nM dimer. G) Anomalous electrophoretic mobility of mutant GabR-DNA complexes formed with a 351 bp DNA fragment harboring the cognate site in the middle (lanes 1, 3) or at the end (lanes 2, 4). Lanes 1 and 2 GabR R129Q; lanes 3 and 4 GabR K362.366Q.

Figure 8. Proposed model of the GabR-DNA interaction. A) Side view of the complex with the GabR AT-fold domains and wHTH DNA-binding domains in orange and green, respectively. The curved DNA (80° bending) is shown in gray with the direct repeats in red. B) Top view of the complex shown in A. C) Top view of the complex shown in A highlighting the electrostatic potential surface of GabR. D) Enlarged view of the AT domain-DNA interaction obtained from the docking showing the possible interaction of lysine and arginine residues with the DNA phosphates and the TGGTAC inverted sequence shown in blue.

Table3

Table 1. Counts, geometric parameters, occupancy and *K*d of GabR-DNA complexes imaged by AFM under different conditions.

Type of complex	Total DNA	N. Specific complexes	N. aspecific complexes	Height (nm)	Perimeter (nm)	Surface area (nm^2)	Volume (nm^3)	Occupancy (%)	*K*d (nM)
holo-GabR/*gabTD*	1601	619	156	1.7 ± 0.4	53 ± 7	275 ± 56	260 ± 68	38.6 ± 0.9	10 ± 1
holo-GabR-GABA/*gabTD*	2738	553	178	1.5 ± 0.4	59 ± 8	324 ± 67	276 ± 83	20.2 ± 0.7	24 ± 1
apo-GabR/*gabTD*	1334	493	91	1.9 ± 0.5	52 ± 6	276 ± 48	284 ± 77	36.9 ± 2.3	11 ± 1
holo-GabR/*gabTDsub1*	1471	486	98	1.5 ± 0.5	62 ± 8	361 ± 75	278 ± 88	33.0 ± 0.1	13 ± 1
holo-GabR-GABA/*gabTDsub1*	1984	322	95	1.3 ± 0.5	63 ± 6	374 ± 58	252 ± 66	16.2 ± 0.6	33 ± 1
holo-GabR/*gabTDsub2*	1988	283	126	1.6 ± 0.3	62 ± 5	372 ± 52	290 ± 77	14.2 ± 1.3	35 ± 1
holo-GabR-GABA/*gabTDsub2*	2086	139	107	1.7 ± 0.6	57 ± 6	308 ± 50	267 ± 94	6.6 ± 0.1	67 ± 2
holo-GabR/*gabTDsub3*	3086	171	102	1.7 ± 0.4	61 ± 6	361 ± 57	290 ± 85	5.5 ± 0.9	95 ± 8
holo-GabR-GABA/*gabTDsub3*	1733	40	39	1.5 ± 0.4	59 ± 6	328 ± 56	251 ± 78	2.3 ± 0.6	187 ± 29
holo-GabR/*gabTDins5*	1359	66	87	1.5 ± 0.6	65 ± 10	379 ± 89	307 ± 121	4.8 ± 1.0	72 ± 3
holo-GabR/*gabTDins10*	614	196	78	1.2 ± 0.3	62 ± 9	350 ± 72	253 ± 56	31.8 ± 1.8	12 ± 1
GabR R129Q/*gabTD*	2179	718	142	1.3 ± 0.5	65 ± 10	390 ± 96	264 ± 85	32.9 ± 0.9	22 ± 1
GabR K362.366Q/*gabTD*	2252	131	100	1.4 ± 0.5	64 ± 8	364 ± 68	267 ± 100	5.8 ± 0.4	252 ± 31

When present, GABA concentration was 10 mM. Total DNA represents the number of bound and unbound DNA molecules in the images. Specific complexes are those with an arm ratio in the range 0.50 - 0.80, while non-specific complexes are those with an arm ratio outside this range. Height, perimeter, surface area and volume values are given as mean ±SD. The occupancy is obtained from the ratio between the number of specific complexes and the total number of DNA. The dissociation constant (*K*d) with respect to the concentration of GabR dimer was determined as described in the text. Values are given ±SD of three independent experiments. GabR concentration was 87.5 nM in all cases except for R129Q (140 nM) and K362.366Q (280 nM).

Supplementary Table 1. Primers used in this study.

Primers	**Sequence 5'–3'**	**Constructs**
GabR-for GabR-rev	AATATAAAGGTCTCAAATGGATATCACGATTACACTC ATAATTGGTCTCAGCGCTATCCCCTGTAACGGGG	pASK-GabR
GabR-R129Q-for GabR-R129Q-rev	CTGGTTCCAGTGCGAGCAAAAAG CTTTTTGCTCGCACTGGAACCAG	pASK-GabR-R129Q
GabR-K362-366Q-for GabR-K362-366Q-rev	GAATATCAGCAGCATATAAAACAAATGAAGC GCTTCATTTGTTTTATATGCTGCTGATATTC	pASK-GabR-K362-366Q
GabTD-for (*) GabTD-rev (*)	ATATGAATTCTCCGGCCATCCAGATC ATATGAATTCTGAATTT ACGCTGACC	pNEB-*gabTD*
GabTD-ins5-for (**) GabTD-ins5-rev (**)	ATGAAAAGTACCCATGGAATTATAACTTTTTGATGGTATC ATAATTCCATGGGTACTTTTCATCATACCAAAG	pNEB-*gabTDIns5*
GabTD-ins10-for (**) GabTD-ins10-rev (**)	AAGTACCCATGGATGCTAATTATAACTTTTTGATGGTATC TAATTAGCATCCATGGGTACTTTTCATCATAC	pNEB-*gabTDIns10*
GabTD-sub1-for (**) GabTD-sub1-rev (**)	GATGAAAAGTTATAATTATAACTTTTTG CAAAAAGTTATAATTATAACTTTTCATC	pNEB-*gabTDsub1*
GabTD-sub2-for (**) GabTD-sub2-rev (**)	GACTTCTCTTTATCATGATGAAAAG CTTTTCATCATGATAAAGAGAAGTC	pNEB-*gabTDsub2*
GabTD-sub2-for (**) GabTD-sub2-rev (**)	GACTTCTCTTTATCATGATGAAAAG CTTTTCATCATGATAAAGAGAAGTC	pNEB-*gabTDsub3*
GabTD-800-for GabTD-800-rev	TTGGCGGGTGTCGGGGCTG CACAGGAAACAGCTATGACC	DNA fragments used in AFM
PgabRTD-for PgabRTD-rev	GTTCTGAACGATCGAGTGTAATC ATGCTTGCTGTTGTTTGACTC	DNA fragments used in EMSA
GabRbsmiddle_for GabRbsmiddle_rev	CCAGCTCCCGCTTGGAGGG CTCCTTTGACCGCCAGACTG	DNA fragments for DNA bend angle determination
GabRbsend2_for GabRbsend2_rev	CAGGAAACAGCTATGACCATG TCTCCTTCTGATACCATCAAAAAG	DNA fragments for DNA bend angle determination

(*) flanking primers; (**) internal primers. Underlined sequences indicate insertion or substitution of bp in the wt *gabTD* promoter.

Supplementary Table 2. Score parameters of the GabR-DNA docking simulation

CLUSTER 4	
HADDOCK score	-20.7 ± 19.6
Cluster size	7
RMSD from the overall lowest-energy structure	7.4 ± 0.2
Van der Waals energy	-41.5 ± 8.4
Electrostatic energy	-1316.8 ± 80.4
Desolvation energy	205.5 ± 16.0
Restraints violation energy	787.0 ± 25.25
Buried Surface Area	2696.3 ± 285.9
Z-Score	-0.5

Figures

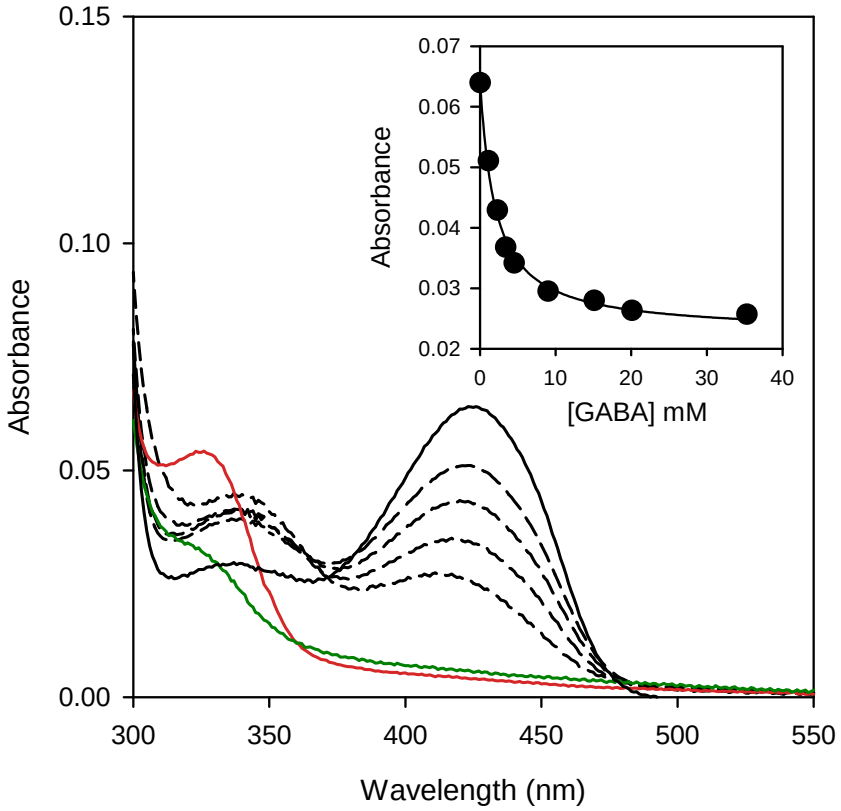

Figure 1

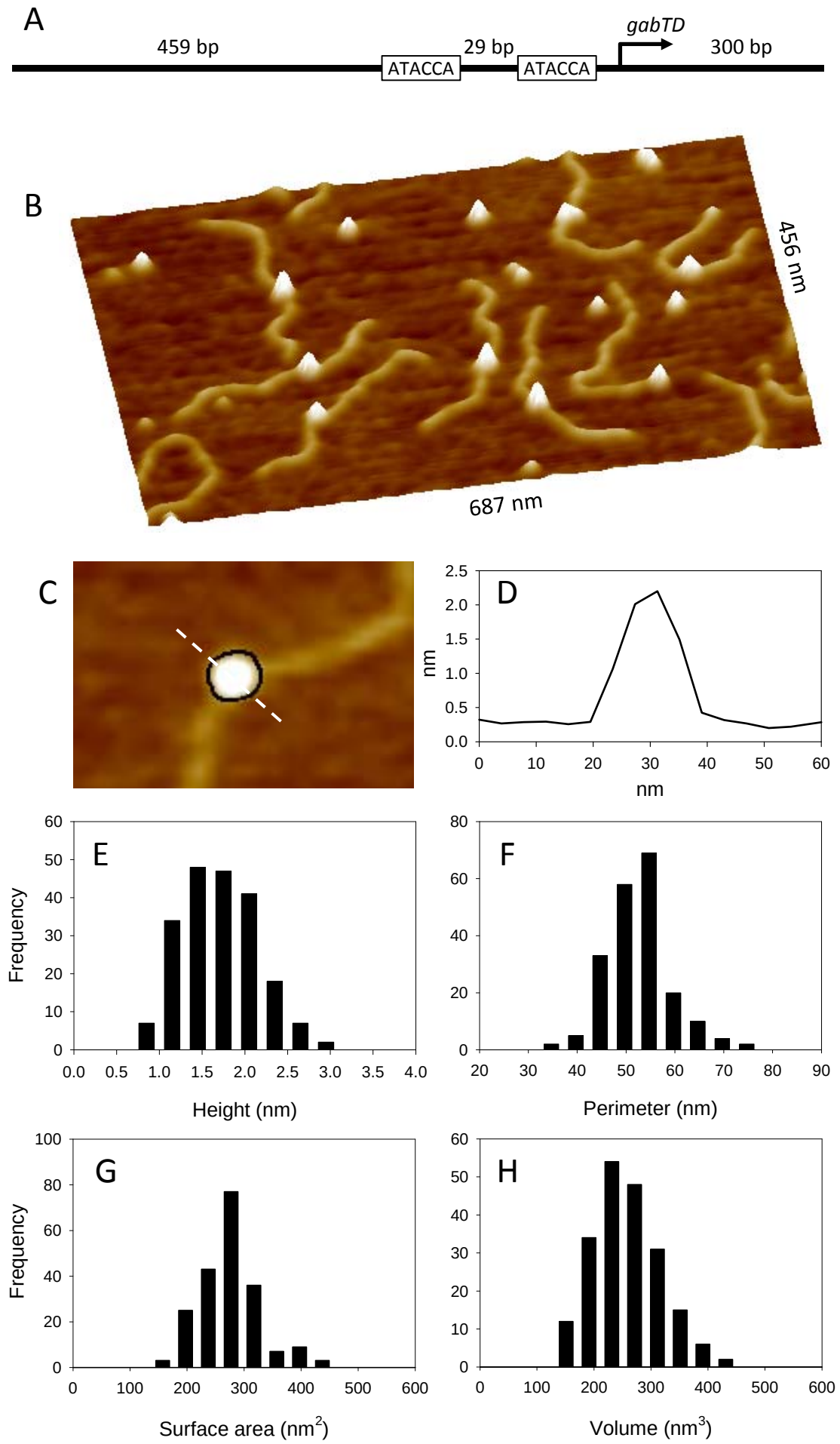
A
459 bp
ATACCA
29 bp
ATACCA
gabTD
300 bp
B
456 nm
687 nm
C
D
nm
nm
E
Frequency
Height (nm)
F
Perimeter (nm)
G
Frequency
Surface area (nm2)
H
Volume (nm3)

Figure 2

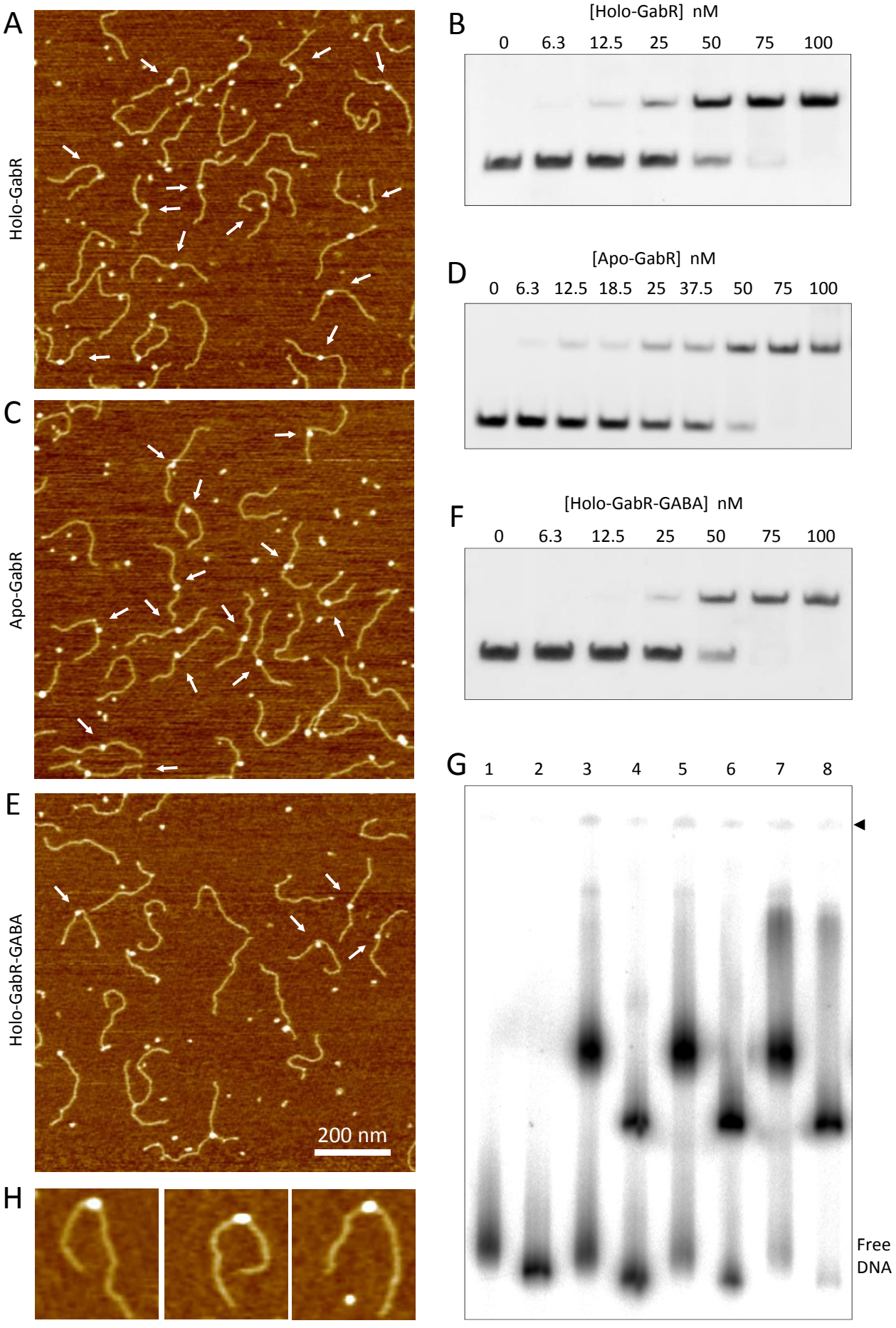
A
Holo-GabR
B
[Holo-GabR] nM
0 6.3 12.5 25 50 75 100
C
Apo-GabR
D
[Apo-GabR] nM
0 6.3 12.5 18.5 25 37.5 50 75 100
E
Holo-GabR-GABA
F
[Holo-GabR-GABA] nM
0 6.3 12.5 25 50 75 100
200 nm
G
1 2 3 4 5 6 7 8
Free DNA
H

Figure 3

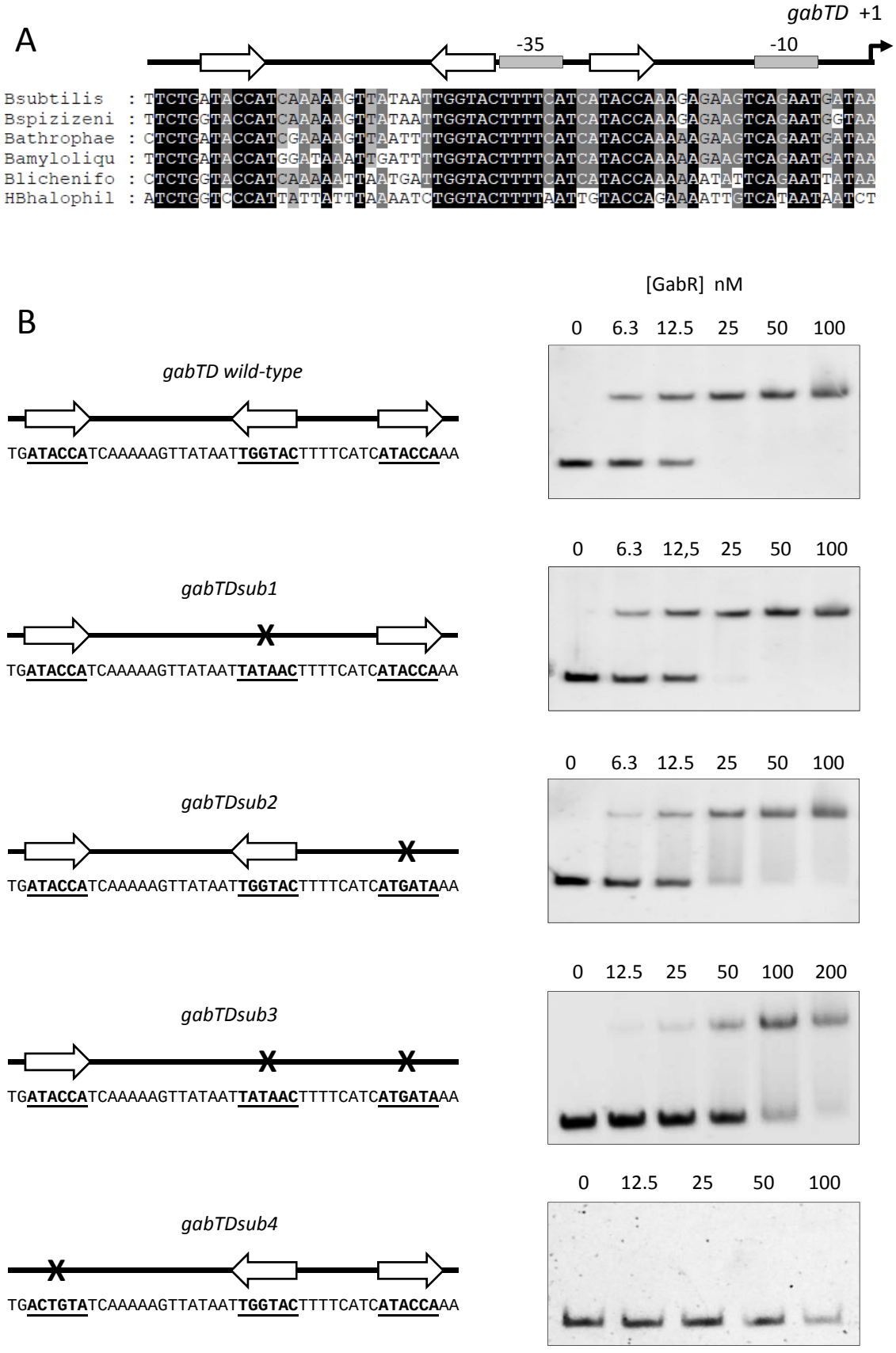
A
gabTD +1
-35
-10
Bsubtilis : TTCTGATACCATCAAAAAGTTATAATTGGTACTTTTCATCATACCAAAGAGAAGTCAGAATGATAA
Bspizizeni : TTCTGGTACCATCAAAAAGTTATAATTGGTACTTTTCATCATACCAAAGAGAAGTCAGAATGGTAA
Bathrophae : CTCTGATACCATCGAAAAGTTAATTTTGGTACTTTTCATCATACCAAAAAGAAGTCAGAATGATAA
Bamyloliqu : TTCTGATACCATGGATAAATTGATTTTGGTACTTTTCATCATACCAAAAAGAAGTCAGAATGATAA
Blichenifo : CTCTGGTACCATCAAAAATTAATGATTGGTACTTTTCATCATACCAAAAAAATATTCAGAATTATAA
HBhalophil : ATCTGGTCCCATTATTATTTAAAATCTGGTACTTTTAATTGTACCAGAAAATTGTCATAATAATCT
B
[GabR] nM
gabTD wild-type
TGATACCATCAAAAAGTTATAATTGGTACTTTTCATCATACCAAA
0 6.3 12.5 25 50 100
gabTDsub1
TGATACCATCAAAAAGTTATAATTATAACTTTTCATCATACCAAA
0 6.3 12,5 25 50 100
gabTDsub2
TGATACCATCAAAAAGTTATAATTGGTACTTTTCATCATGATAAA
0 6.3 12.5 25 50 100
gabTDsub3
TGATACCATCAAAAAGTTATAATTATAACTTTTCATCATGATAAA
0 12.5 25 50 100 200
gabTDsub4
TGACTGTATCAAAAAGTTATAATTGGTACTTTTCATCATACCAAA
0 12.5 25 50 100

Figure 4

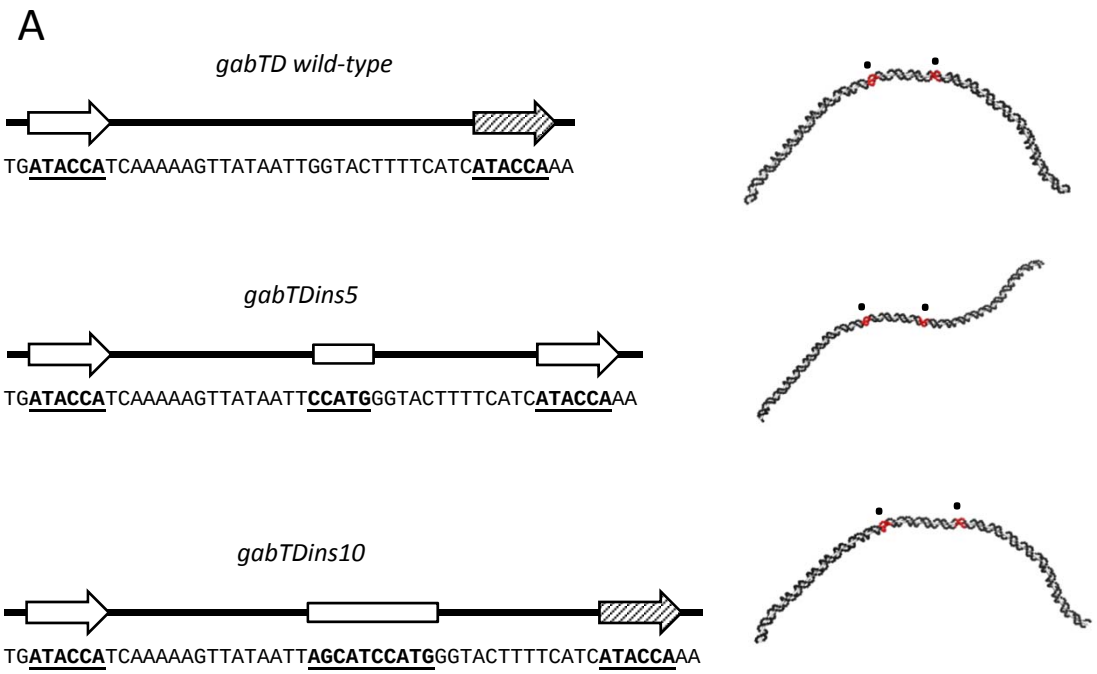
A
gabTD wild-type
TGATACCATCAAAAAGTTATAATTGGTACTTTTCATCATACCAAA
gabTDins5
TGATACCATCAAAAAGTTATAATTCCATGGGTACTTTTCATCATACCAAA
gabTDins10
TGATACCATCAAAAAGTTATAATTAGCATCCATGGGTACTTTTCATCATACCAAA

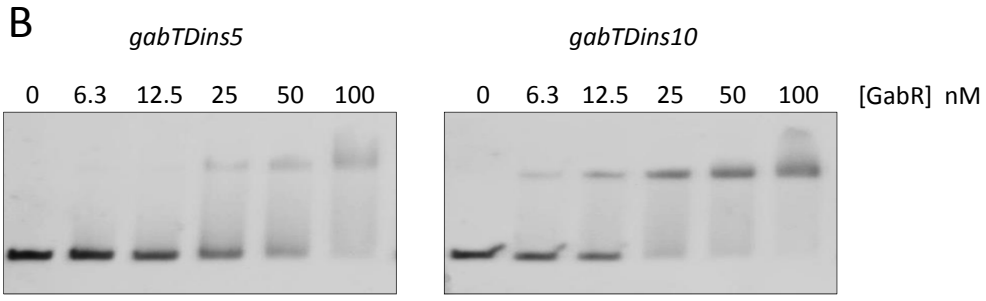
B
gabTDins5
gabTDins10
0 6.3 12.5 25 50 100
0 6.3 12.5 25 50 100
[GabR] nM

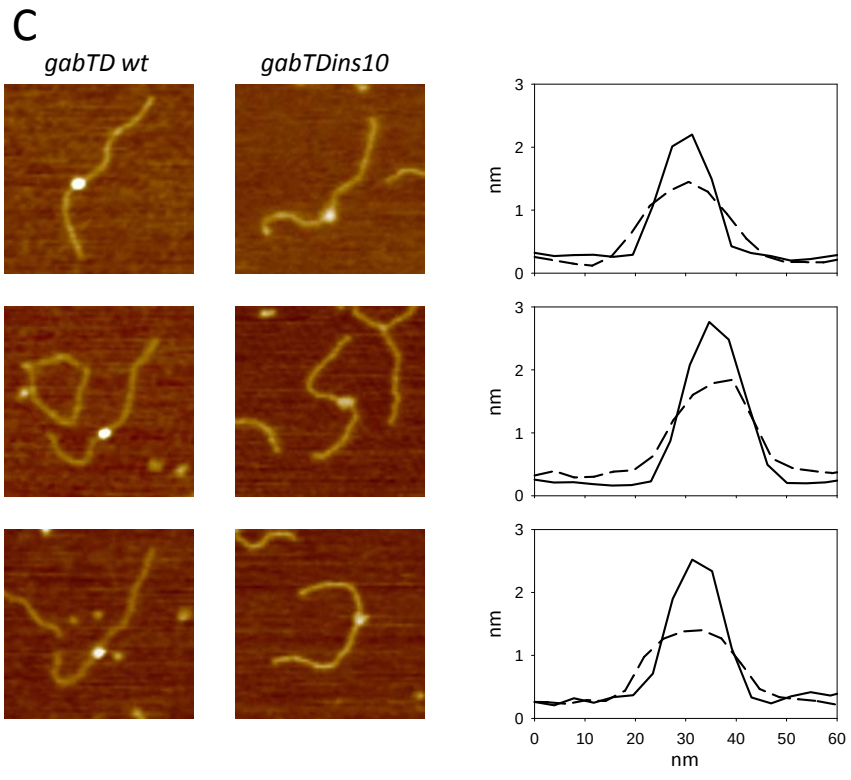
C
gabTD wt
gabTDins10
nm
nm
nm
0 10 20 30 40 50 60
nm

Figure 5

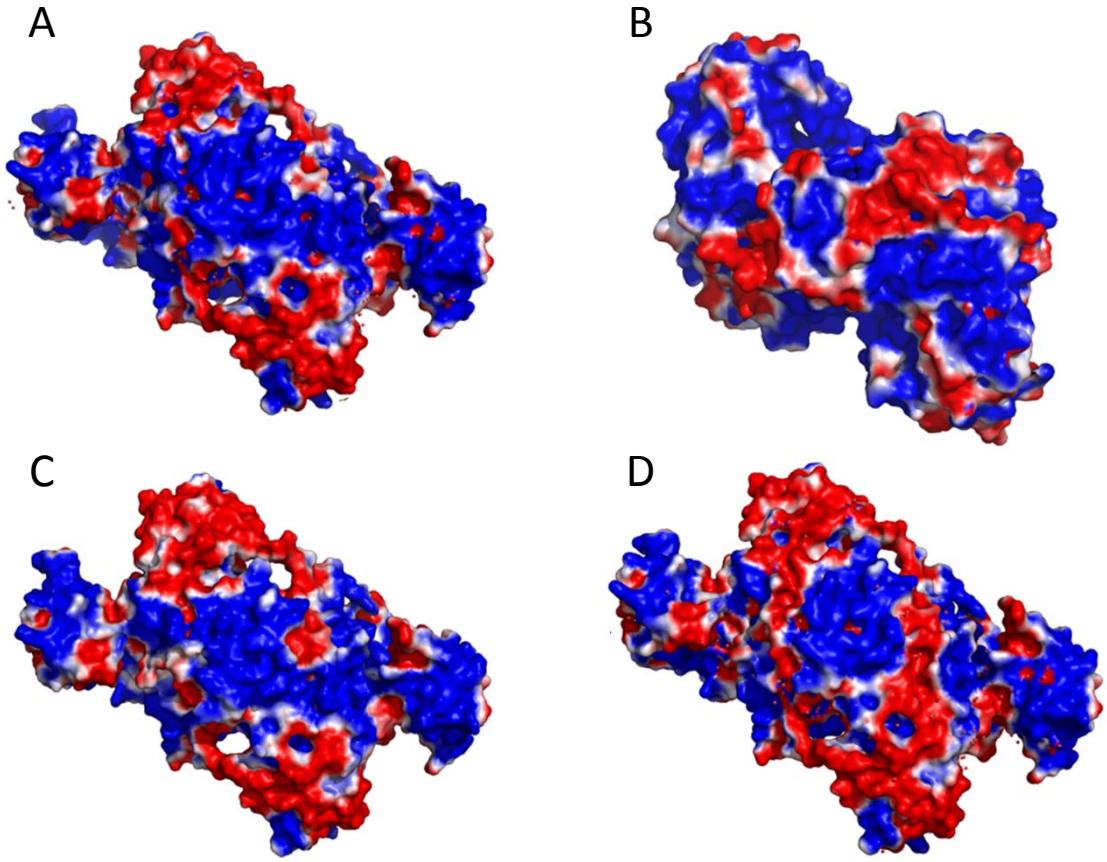

Figure 6

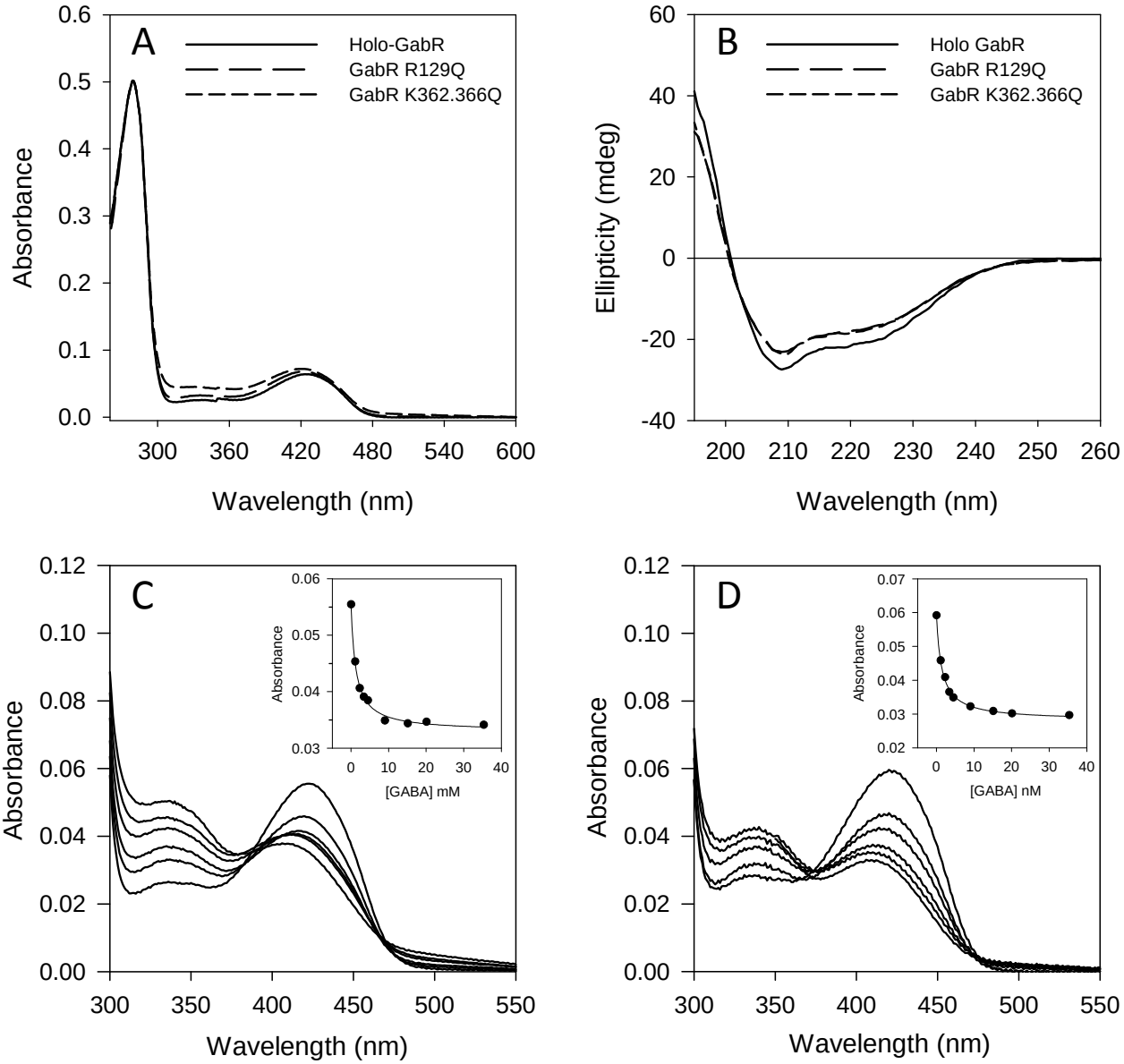
A
Holo-GabR
GabR R129Q
GabR K362.366Q
Absorbance
Wavelength (nm)
B
Holo GabR
GabR R129Q
GabR K362.366Q
Ellipticity (mdeg)
Wavelength (nm)
C
Absorbance
[GABA] mM
Absorbance
Wavelength (nm)
D
Absorbance
[GABA] nM
Absorbance
Wavelength (nm)

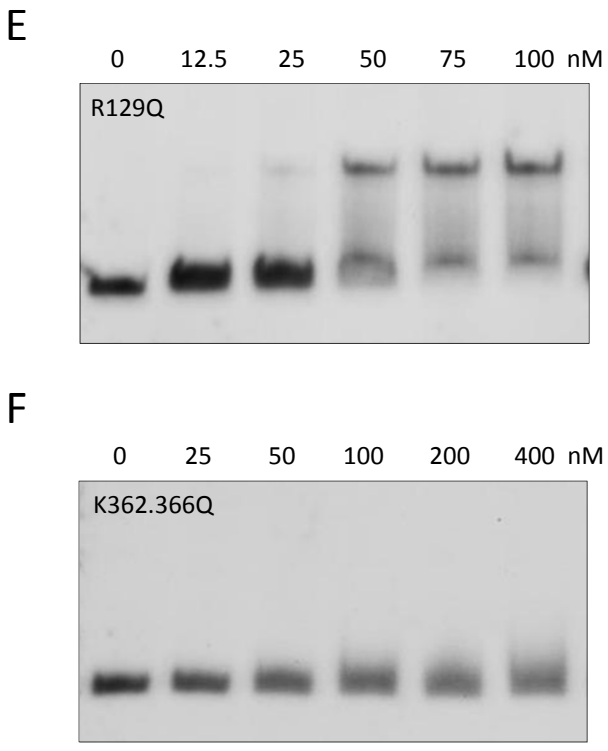
E
0 12.5 25 50 75 100 nM
R129Q
F
0 25 50 100 200 400 nM
K362.366Q

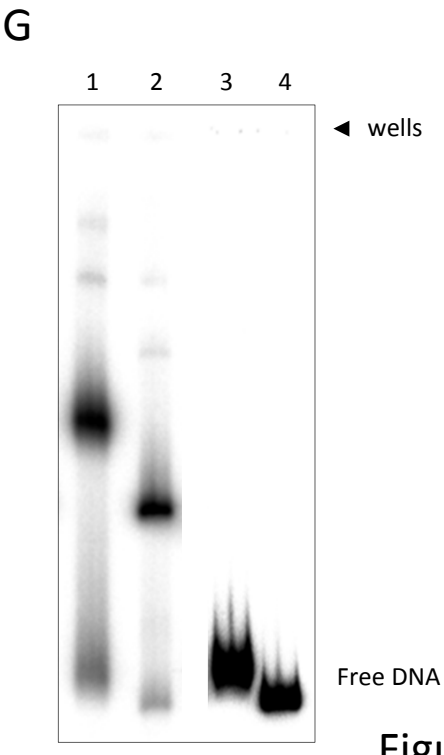
G
1 2 3 4
wells
Free DNA

Figure 7

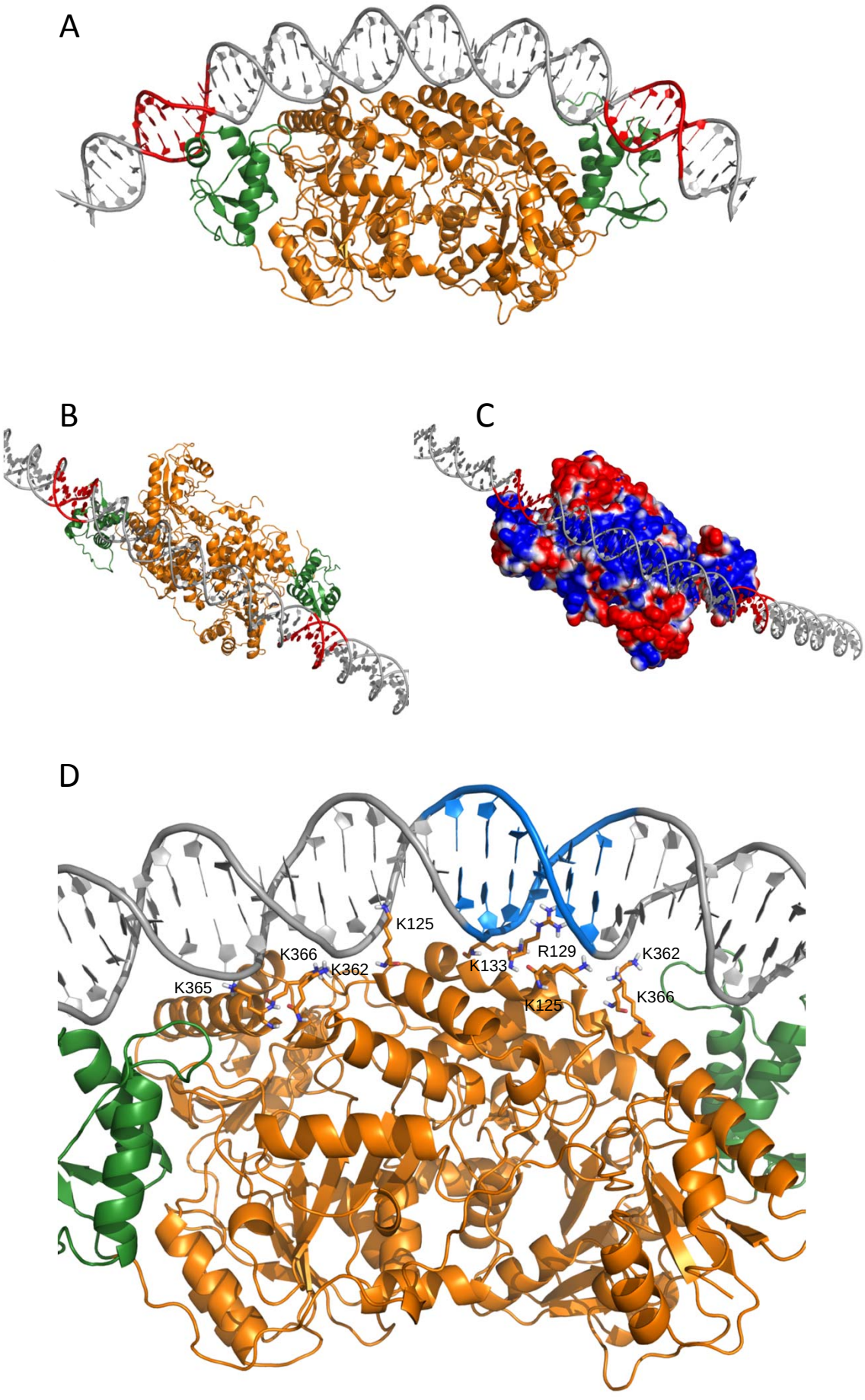

Figure 8

Supplementary Material (for online publication)

Click here to download Supplementary Material (for online publication): Supplementary.pdf

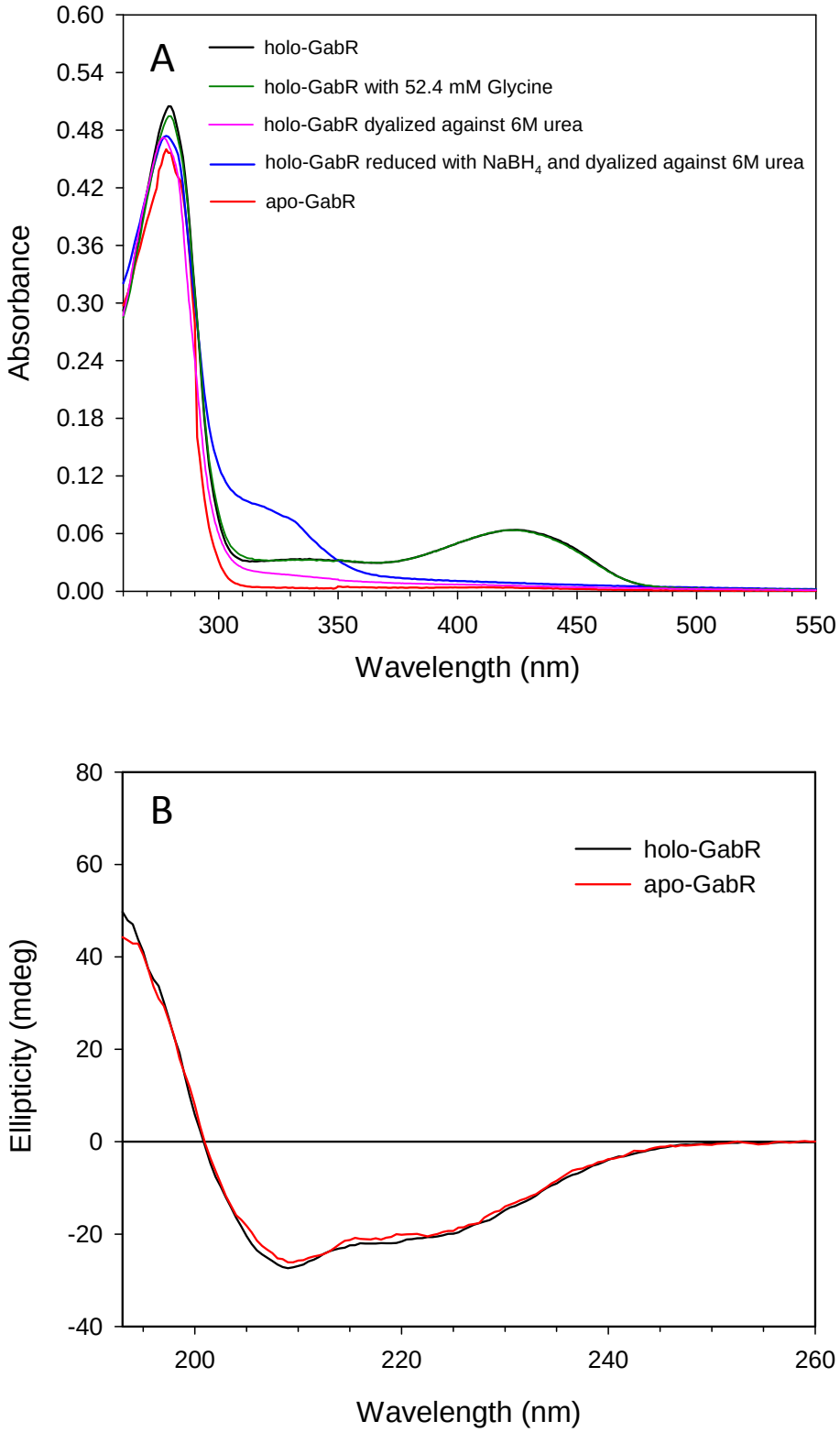

Supplementary Figure S1. A) Absorption spectra of holo-GabR, holo-GabR in the presence of 52.4 mM Glycine, holo-GabR after O/N dialysis against 6M urea, holo-GabR reduced by $NaBH_4$ after O/N dialysis against 6M urea and apo-GabR. Spectra were collected from a solution containing 15 µM GabR in storage buffer at 25 °C. B) Circular dichroism spectra of holo- and apo-GabR.

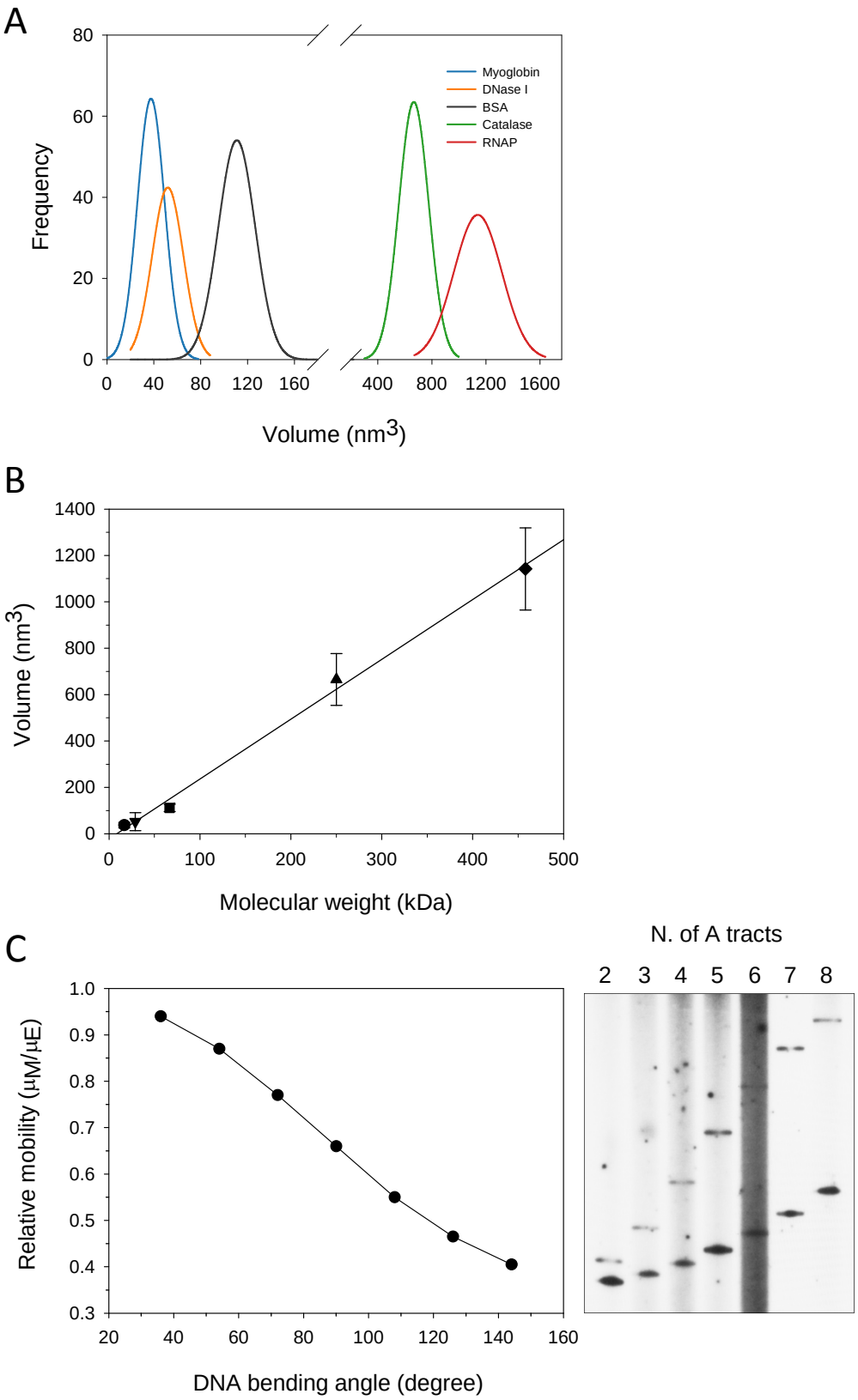

Supplementary Figure S2. Molecular mass calibration curve. A) Volume distributions determined by AFM of five globular proteins with known molecular mass. From left to right: Myoglobin (16.7 kDa), DNase I (29 kDa), BSA (66.7 kDa), Catalase (250 kDa) and *E. coli* RNA polymerase-σ^{70} (458 kDa). B) The mean of each volume distribution is plotted against the molecular mass of the protein. The error bars are the standard deviation of the distributions shown in panel A. C) Relative electrophoretic mobility of DNA fragments containing from two to eight phased A tracts (gel shown on the right). An angle of 18° for each A tract has been assumed based on crystallographic and gel mobility data (Thompson JF and Landy A 1988 Nucleic Acids Res 9687; Nelson HCM, Finch JT, Luisi BF and Klug A 1987 Nature 221).

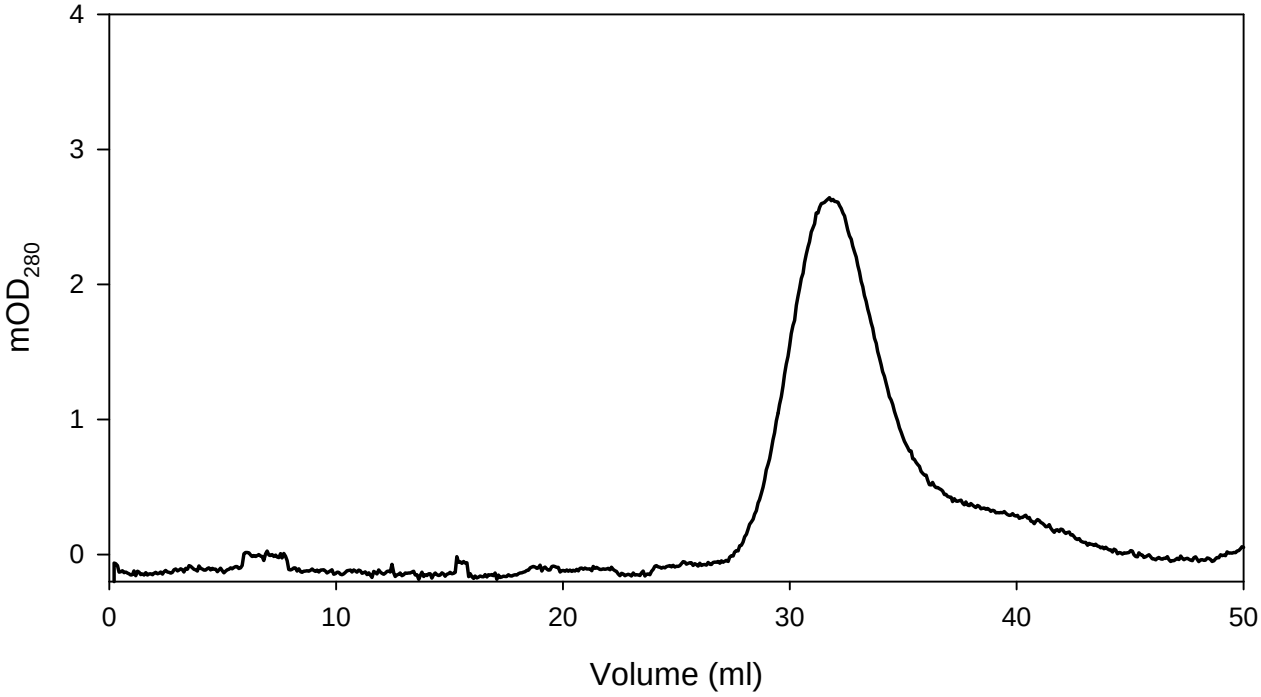

Supplementary Figure S3. Size exclusion chromatography elution profile of holo-GabR. The elution peak centered at 31 ml represents the dimeric holo-GabR (112 kDa). See Materials and Methods for calibration details.

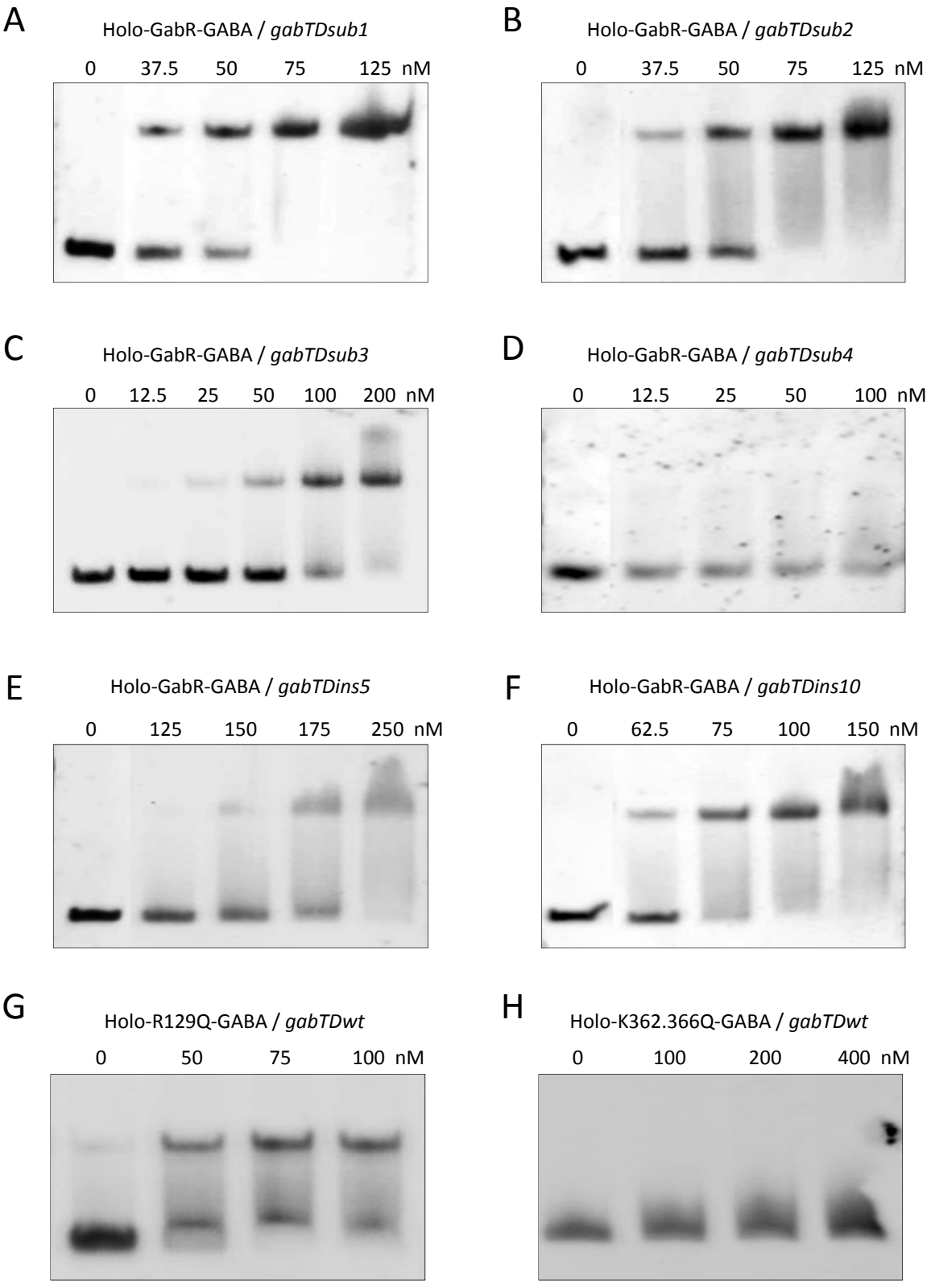

Supplementary Figure S4. Effect of GABA on GabR-DNA binding investigated by polyacrylamide gel mobility-shift assay. Holo-GabR-GABA with DNA fragments harboring different mutant promoters *gabTDsub1* (A), *gabTDsub2* (B), *gabTDsub3* (C), *gabTDsub4* (D), *gabTDins5* (E) and *gabTDins10* (F). Holo-GabR(R129Q)-GABA (G) and holo-GabR(K362.366Q)-GABA (H) with a DNA fragment harboring the *wt gabTD* promoter. In all experiments GabR was incubated with a saturating concentration of GABA (20 mM) prior to the addition of DNA. Gels were stained with SYBR Green.

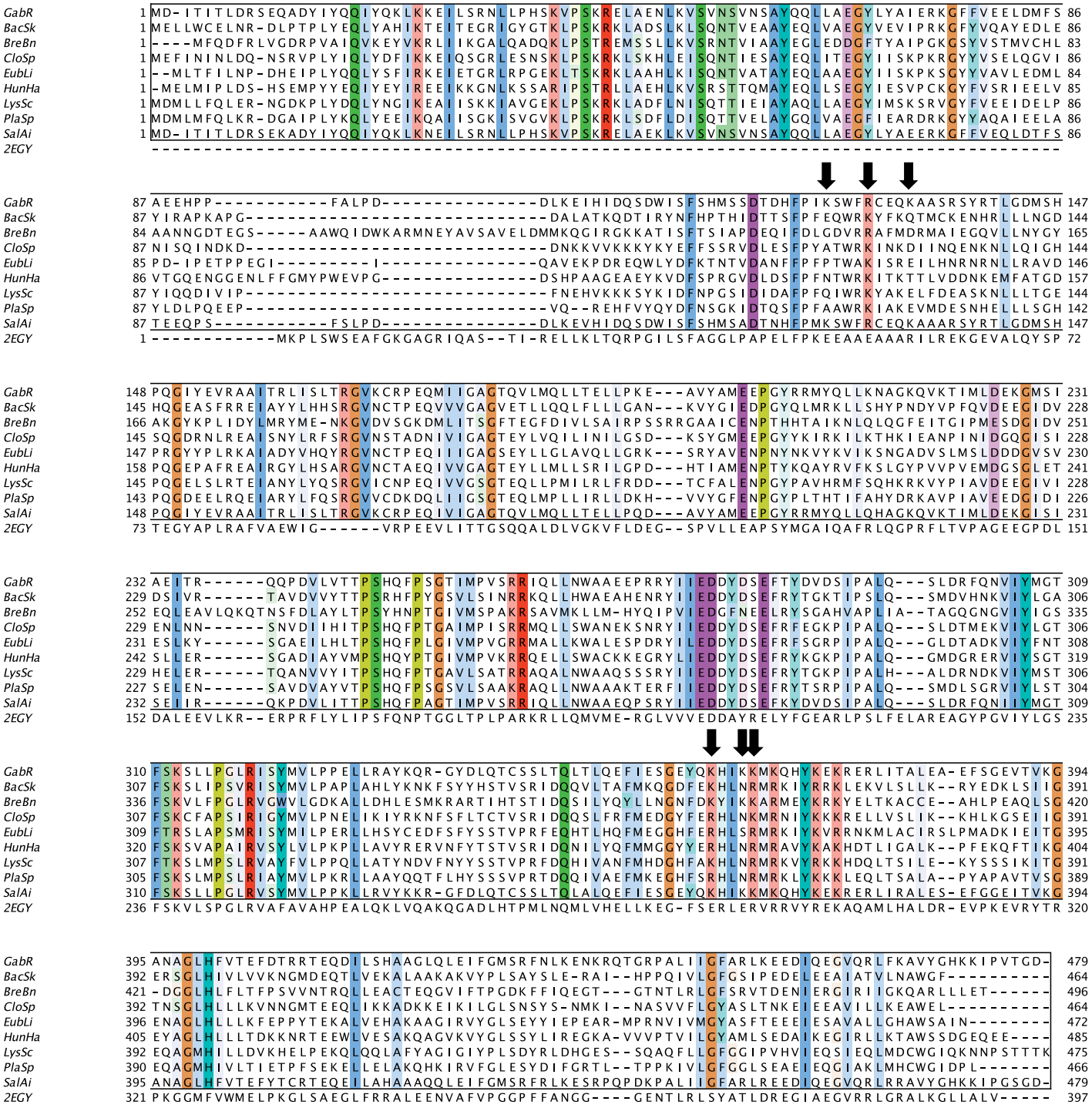

Supplementary Figure S5 Multiple sequence alignment of GabR, representative MocR members and *Thermus thermophilus* 2-aminoadipate aminotransferase.

From top to bottom: GabR (*Bacillus subtilis* Uniprot ID P94426); BacSk (*Bacillus clausii* Uniprot ID Q5WKW3); BreBn (*Brevibacillus brevis* Uniprot ID C0ZDG2); CloSp (*Clostridium sp*. Uniprot ID V9H8E1); EubLi (*Eubacterium limosum* Uniprot ID E3GR75); HunHa (*Clostridia bacterium* Uniprot ID UPI0004955FF1); LysSc (*Lysinibacillus sphaericus* Uniprot ID B1HS44); PlaSp (*Planomicrobium sp*. Uniprot ID A0A098EIQ0); SalAi (*Salinibacillus aidingensis* Uniprot ID UPI00039C6A7C); 2EGY 2-aminoadipate aminotransferase (*Thermus Thermophilus* Uniprot ID Q72LL6). Residues with a conservation of their physico-chemical properties higher than 80% are colored. Black arrows indicate the basic residues discussed in the text.

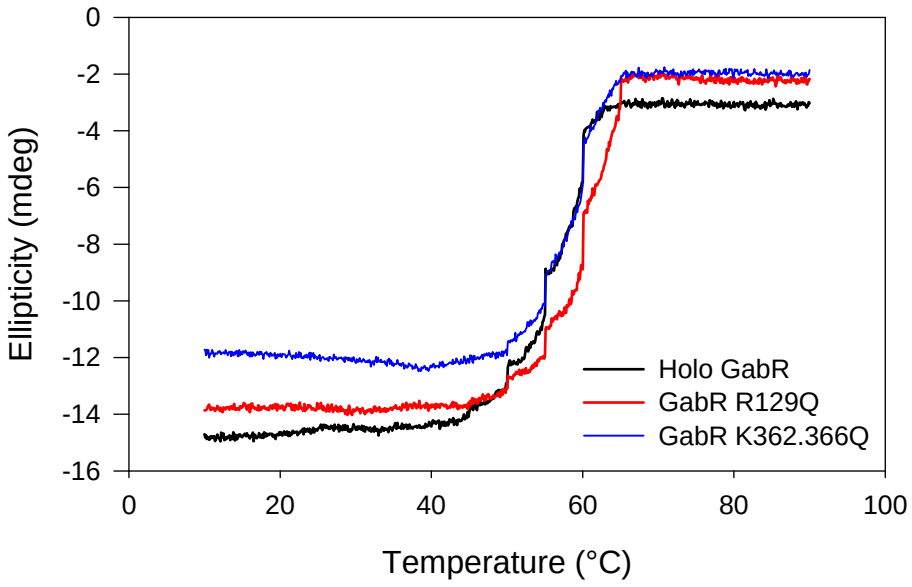

Supplementary Figure S6. Thermal denaturation curves of wt GabR, GabR R129Q and GabR K362.366Q.

Supplementary Table 1. Primers used in this study.

Primers	**Sequence 5'–3'**	**Constructs**
GabR-for GabR-rev	AATATAAAGGTCTCAAATGGATATCACGATTACACTC ATAATTGGTCTCAGCGCTATCCCCTGTAACGGGG	pASK-GabR
GabR-R129Q-for GabR-R129Q-rev	CTGGTTCCAGTGCGAGCAAAAAG CTTTTTGCTCGCACTGGAACCAG	pASK-GabR-R129Q
GabR-K362-366Q-for GabR-K362-366Q-rev	GAATATCAGCAGCATATAAAACAAATGAAGC GCTTCATTTGTTTTATATGCTGCTGATATTC	pASK-GabR-K362-366Q
GabTD-for (*) GabTD-rev (*)	ATATGAATTCTCCGGCCATCCAGATC ATATGAATTCTGAATTT ACGCTGACC	pNEB-*gabTD*
GabTD-ins5-for (**) GabTD-ins5-rev (**)	ATGAAAAGTACCCATGGAATTATAACTTTTTGATGGTATC ATAATTCCATGGGTACTTTTCATCATACCAAAG	pNEB-*gabTDIns5*
GabTD-ins10-for (**) GabTD-ins10-rev (**)	AAGTACCCATGGATGCTAATTATAACTTTTTGATGGTATC TAATTAGCATCCATGGGTACTTTTCATCATAC	pNEB-*gabTDIns10*
GabTD-sub1-for (**) GabTD-sub1-rev (**)	GATGAAAAGTTATAATTATAACTTTTTG CAAAAAGTTATAATTATAACTTTTCATC	pNEB-*gabTDsub1*
GabTD-sub2-for (**) GabTD-sub2-rev (**)	GACTTCTCTTTATCATGATGAAAAG CTTTTCATCATGATAAAGAGAAGTC	pNEB-*gabTDsub2*
GabTD-sub2-for (**) GabTD-sub2-rev (**)	GACTTCTCTTTATCATGATGAAAAG CTTTTCATCATGATAAAGAGAAGTC	pNEB-*gabTDsub3*
GabTD-800-for GabTD-800-rev	TTGGCGGGTGTCGGGGCTG CACAGGAAACAGCTATGACC	DNA fragments used in AFM
PgabRTD-for PgabRTD-rev	GTTCTGAACGATCGAGTGTAATC ATGCTTGCTGTTGTTTGACTC	DNA fragments used in EMSA
GabRbsmiddle_for GabRbsmiddle_rev	CCAGCTCCCGCTTGGAGGG CTCCTTTGACCGCCAGACTG	DNA fragments for DNA bend angle determination
GabRbsend2_for GabRbsend2_rev	CAGGAAACAGCTATGACCATG TCTCCTTCTGATACCATCAAAAAG	DNA fragments for DNA bend angle determination

(*) flanking primers; (**) internal primers. Underlined sequences indicate insertion or substitution of bp in the wt *gabTD* promoter.

Supplementary Table 2. Score parameters of the GabR-DNA docking simulation

CLUSTER 4	
HADDOCK score	-20.7 ± 19.6
Cluster size	7
RMSD from the overall lowest-energy structure	7.4 ± 0.2
Van der Waals energy	-41.5 ± 8.4
Electrostatic energy	-1316.8 ± 80.4
Desolvation energy	205.5 ± 16.0
Restraints violation energy	787.0 ± 25.25
Buried Surface Area	2696.3 ± 285.9
Z-Score	-0.5